

Article

Inverse ISAsomes in Bio-Compatible Oils—Exploring Formulations in Squalane, Triolein and Olive Oil

Florian Trummer [†], Otto Glatter  and Angela Chemelli ^{*}

Institute of Inorganic Chemistry, Faculty of Technical Chemistry, Chemical and Process Engineering, Biotechnology, Graz University of Technology, Stremayrgasse 9, 8010 Graz, Austria; florian.trummer@uibk.ac.at (F.T.); otto.glatter@tugraz.at (O.G.)

* Correspondence: angela.chemelli@tugraz.at

[†] Current address: Institute for Ion Physics and Applied Physics, Faculty of Mathematics, Computer Science and Physics, University of Innsbruck, Technikerstraße 25, 6020 Innsbruck, Austria.

Abstract: In contrast to their more common counterparts in aqueous solutions, inverse ISAsomes (internally self-assembled somes/particles) are formulated as kinetically stabilised dispersions of hydrophilic, lyotropic liquid-crystalline (LC) phases in non-polar oils. This contribution reports on their formation in bio-compatible oils. We found that it is possible to create inverse hexosomes, inverse micellar cubosomes (Fd3m) and an inverse emulsified microemulsion (EME) in excess squalane with a polyethylene glycol alkyl ether as the primary surfactant forming the LC phase and to stabilise them with hydrophobised silica nanoparticles. Furthermore, an emulsified L_1 -phase and inverse hexosomes were formed in excess triolein with the triblock-copolymer Pluronic[®] P94 as the primary surfactant. Stabilisation was achieved with a molecular stabiliser of type polyethylene glycol (PEG)-dipolyhydroxystearate. For the inverse hexosomes in triolein, the possibility of a formulation without any additional stabiliser was explored. It was found that a sufficiently strong stabilisation effect was created by the primary surfactant alone. Finally, triolein was replaced with olive oil which also led to the successful formation of inverse hexosomes. As far as we know, there exists no previous contribution about inverse ISAsomes in complex oils such as triolein or plant oils, and the existence of stabiliser-free (i.e., self-stabilising) inverse hexosomes has also not been reported until now.

Keywords: ISAsomes; inverse cubosomes; inverse hexosomes; self-assembly; nanostructures



Citation: Trummer, F.; Glatter, O.; Chemelli, A. Inverse ISAsomes in Bio-Compatible Oils—Exploring Formulations in Squalane, Triolein and Olive Oil. *Nanomaterials* **2022**, *12*, 1133. <https://doi.org/10.3390/nano12071133>

Academic Editor: Angelina Angelova

Received: 12 January 2022

Accepted: 28 March 2022

Published: 29 March 2022

Publisher's Note: MDPI stays neutral with regard to jurisdictional claims in published maps and institutional affiliations.



Copyright: © 2022 by the authors. Licensee MDPI, Basel, Switzerland. This article is an open access article distributed under the terms and conditions of the Creative Commons Attribution (CC BY) license (<https://creativecommons.org/licenses/by/4.0/>).

1. Introduction

Upon increased addition of amphiphilic molecules to an aqueous solution, hydrophobic forces will lead to the formation of aggregates that are known as micelles—the concentration threshold where micelles start to form is referred to as the critical micelle concentration [1–5]. When the concentration of amphiphilic molecules is further increased, the micelles will usually arrange into ordered structures and form lyotropic liquid-crystalline (LC) phases. Amphiphilic molecules, or surfactants, can be classified as ionic or non-ionic, and both types have advantages in certain fields of application [6]. Non-ionic surfactants comprise monoglycerides [7,8], fatty acids [9], phospholipids [10], amphiphilic block-copolymers [11–16] and many other classes of molecules [17].

1.1. ISAsomes—Definition and Nomenclature

Self-assembled LC-phases that are dilutable with an oil phase are usually termed as lipophilic and “inverse”—a term that is derived from the definition of inverse micelles. They comprise the following: inverse bicontinuous cubic phases (V_2), inverse hexagonal phases (H_2), inverse micellar cubic phases (I_2) and inverse micelles/microemulsions (L_2). The subscript 2 denotes that these LC-phases are lipophilic and “inverse”. If lipophilic LC-phases are capable of coexisting with a hydrophilic excess medium (typically water), they can be dispersed and stabilised in said medium, resulting in internally self-assembled,

nanostructured particles [18–26] and are labelled according to the contained nanostructures mentioned above: bicontinuous cubosomes, hexosomes, micellar cubosomes and emulsified microemulsion (EME)) [25,27–29]. The whole family of particles is usually denoted as ISAsomes (internally self-assembled somes/particles) [30]. Due to historic reasons, the existing nomenclature is rather confusing, as “conventional” ISAsomes contain inverse LC-phases, a fact that will be emphasised again in the subsequent definition of the titular “inverse” ISAsomes. For this reason, the authors strongly recommend the use of categorisation “lipophilic/hydrophilic” for LC-phases in order to avoid confusion in this matter. Dispersed lamellar LC-phases form vesicles that are not included in the ISAsome family and are investigated separately [31–33]. For the sake of completeness, it is necessary to mention that amphiphilic molecules may also arrange into aperiodic quasicrystalline lattices and the production of these structures in thermodynamic equilibrium is a non-trivial task [34,35]. To the best of our knowledge, there exist no reports about dispersed quasicrystalline LC-phases that would be a new addition to the ISAsome family.

1.2. Stabilisation Schemes

The dispersed particles have to be stabilised kinetically in a solution with the help of a secondary emulsifier/stabiliser. ISAsomes are usually formulated as oil-continuous particles that are dispersed in an aqueous solution. Their stabilisation is usually achieved with the help of hydrophilic triblock co-polymers ($\text{PEO}_n\text{PPO}_m\text{PEO}_k$) with high molecular weight (also known as poloxamers) and a high hydrophilic-lipophilic balance (HLB) [18,36,37]. Regardless of their hydrophilic character, these stabiliser molecules can interact with the dispersed LC-particles and lead to a change of the internal structure [38–43]. Other known concepts of emulsion stabilisation include the use of polyelectrolyte complexes [44], but there exist no reports about ISAsome stabilisation with this approach. Another popular technique for emulsion/dispersion stabilisation is the formation of Pickering or Ramsden emulsions, where the stabilisation of dispersed droplets is achieved with solid particles that include silica particles, laponite clay particles, latex particles and many others [45–59]. The stabilisation of emulsion/dispersion droplets strongly depends on the hydrophobicity of the solid stabiliser and the phase which is the best solvent for the emulsifying particles will usually be favoured as the external phase [45].

In recent years, more complex Pickering concepts have been introduced by various contributors. Instead of simply adsorbing spherical Pickering particles onto the surface of the emulsified droplets, stabilisation can be achieved by more complex mechanisms such as particle networks, rod-like particles, plate-shaped particles, etc., [60–62]. Food-grade Pickering emulsifiers are of special interest for bio-compatible applications, and various contributions have shown the emulsifying properties of particles based on calcium carbonate, cellulose nanocrystals/nanofibers and others [61,63–67]. In general, W/O (water-in-oil) Pickering emulsions have not been studied as thoroughly as their O/W (oil-in-water) counterpart [68–73]. As of now, no plant-based W/O Pickering emulsifier capable of producing droplet sizes $<10\ \mu\text{m}$ is known to the scientific community [60].

1.3. Applications

Due to their internal structure and large interfacial area, ISAsomes are unique carrier and delivery systems for a variety of hydrophilic, hydrophobic and amphiphilic molecules. Past contributions have shown their ability to encapsulate medical drugs that are used in the treatment of various types of cancer, neurodegenerative diseases and other sufferings [29,74–93]. The dispersed LC can be chosen according to the specific needs of the delivery application and phase transitions can be triggered by changes in pH [89,94–100], light stimulation [101], temperature changes [102], magnetic fields [103] and other external stimuli. In the case of a magnetic trigger, superparamagnetic iron oxide particles are incorporated into the lyotropic LC, and the phase transition can be attributed to the indirect heating of the “magnetocubosomes” by an alternating external magnetic field. In all cases, the phase transition properties may be used for a triggered release of drugs. In the field

of nutritional science, ISAsomes can be used for the encapsulation of nutraceuticals such as natural phenolic antioxidants, curcumin, aromas, catechin and others [104–121]. The pH sensitivity of ISAsomes is of special interest here, as the gastrointestinal tract shows variations of the pH that enable a controlled release of nutrients where they are optimally digested [122,123]. In addition to oral drug delivery, the applicability of ISAsomes or similar systems in transdermal drug delivery has been shown [124–126]. Apart from specific applications, the formation of Lyotropic LCs and ISAsome-like structures during digestion processes are of special interest for nutritional science and biology and help to facilitate a better understanding of the human body [104–107,127] and understanding the processes behind the formation and interaction of these systems is a key element to unlock new applications in return [128,129].

1.4. Definition of Inverse ISAsomes and Research Goals

Until now, only “conventional” ISAsomes have been discussed. As stated, they are kinetically stabilised oil-continuous particles with a confined lipophilic lyotropic LC-phase or microemulsion. This type of system has been investigated in many contributions, and a variety of system compositions is known. Until recently, no reports about an inverse system had been made. In 2018, a reversion of the system was achieved by dispersing a hydrophilic LC with hexagonal nanostructure (H_1 -phase) in an alkane, resulting in the first report of inverse hexosomes [130]. This feat was achieved with a polyethylene glycol alkyl ether and a poloxamer as surfactants and the stabilisation of the dispersion was performed with a PEG-dipolyhydroxystearate with low HLB on one hand and hydrophobised silica nanoparticles on the other. Due to the system composition in excess tetradecane, the applicability of this system in bio-compatible applications is strongly limited, and to the best of our knowledge, no reports about other types of inverse ISAsomes existed until now. Alternative formulations in cosmetics-grade or food-grade oils would allow the development of delivery applications in an oil-continuous environment.

In this contribution, we demonstrate the formulation of inverse ISAsomes in three bio-compatible types of oil with increasing structural complexity. As stated above, inverse ISAsomes are defined as kinetically stabilised dispersions of hydrophilic LC-phases in an excess oil phase. Hydrophilic LC-phases are dilutable with water and comprise: bicontinuous cubic phases (V_1), hexagonal phases (H_1), micellar cubic phases (I_1) and micelles/microemulsions (L_1). To the best of our knowledge, this contribution is the first to report on the existence of inverse micellar cubosomes, an inverse emulsified microemulsions (EME) and an emulsified L_1 -phase, thus adding three new members to the ISAsome family and enabling further research on the development of applications where the bio-compatibility of all ingredients is of utmost importance. For our study, we chose three different oils as excess phase for inverse ISAsomes: squalane, a hydrocarbon that is often used in cosmetics, and triolein, a food-grade triglyceride that can be viewed as a model oil for natural plant oils. The third oil used was commercially available olive oil. As a first step, binary mixtures of a surfactant and water were produced and the appearing hydrophilic LC-phases were characterised with the help of small-angle X-ray scattering (SAXS). Polarisation light microscopy (PLM) was used as an additional tool in cases where SAXS measurements were not sufficient. As a next step, samples at promising surfactant concentration were loaded with increasing amounts of oil to test the compatibility of the LC-phases with the excess phase. The final step was the dispersion of the hydrophilic LCs in excess oil and the stabilisation of the droplets.

Our work was planned and conducted with the intent of providing a first “proof of principle” for the creation of inverse ISAsomes in (bio-)oil phases. For their characterisation, we relied on available in-house techniques. The particle-internal structure was determined with SAXS (or PLM, where needed) and the mean particle size was determined with dynamic light scattering (DLS) or PLM.

2. Materials and Methods

The aim of this contribution was the development of dispersion and stabilisation of hydrophilic lyotropic LC-phases in two natural oils as the excess phase. While the LC-phase was formed by water and a primary surfactant, the stabilisation in excess oil was achieved with the help of a secondary surfactant or Pickering stabilising nanoparticles. Based on another contribution [130], a polyethylene glycol alkyl ether (C_iE_j) and a poloxamer were chosen as primary surfactants. Due to financial restrictions and for better reproducibility in possible future applications, technical-grade chemicals were used.

2.1. Materials

Genapol LA 070 (Clariant AG, Bruckmühl, Germany) was the first primary surfactant used in this study. The surfactant molecules consisted of an alkyl chain with a length of 12–16 carbon atoms and seven ethylene oxide units. Pluronic® PE9400 (in the following referred to as P94) (BASF SE, Ludwigshafen, Germany) was also used for the formation of the hydrophilic LC-phases. P94 is a triblock-copolymer (type A-B-A) consisting of a hydrophobic polyoxypropylene core (47 units) that is flanked by two hydrophilic polyoxyethylene blocks (21 units each). The chemical structures of both surfactants are shown in Figure 1. For the excess oil phase, three different oils were chosen: squalane (96% purity; Sigma-Aldrich Corp., Burlington, MA, USA) is a hydrocarbon often used in cosmetics. Recent studies have explored its applicability for transdermal delivery applications [126]. Triolein (90% purity; abcr GmbH, Karlsruhe, Germany) is a food-grade triglyceride found in many plant-based natural oils. It was used as a highly purified model oil to investigate the possibility to formulate inverse ISAsomes in commercially available food-grade oils (olive oil, etc.). Commercially available olive oil was the third oil used in this study. The chemical structures of triolein and squalane are shown in Figure 2.

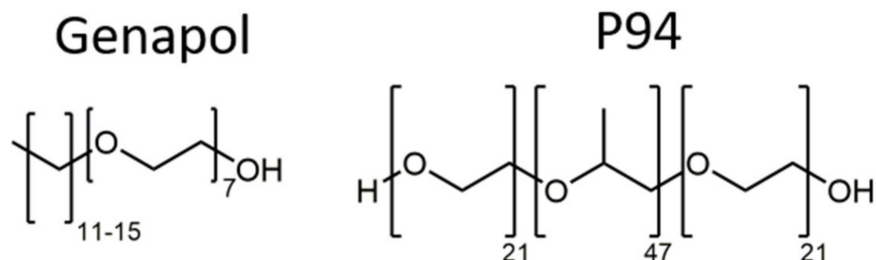


Figure 1. Chemical structures of the primary surfactants Genapol and P94.

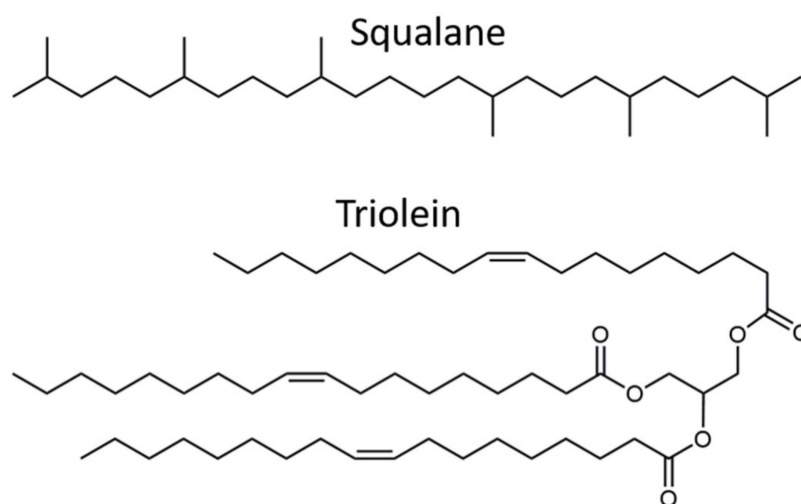


Figure 2. Chemical structures of the oils squalane and triolein.

PEG-30 dipolyhydroxystearate (Cithrol DPHS from Croda International plc, Snaith, UK) was used as molecular stabiliser based on reports about its capability to form stable W/O emulsions in triolein and other oils and contributions that centre around its applicability for oral drug delivery [131,132]. Its chemical structure is shown in Figure 3. Hydrophobised silica nanoparticles of type Aerosil R711 (Evonik Industries AG, Essen, Germany) were used as Pickering- stabilisers for the formation of dispersions. Deionised water was used for all experiments.

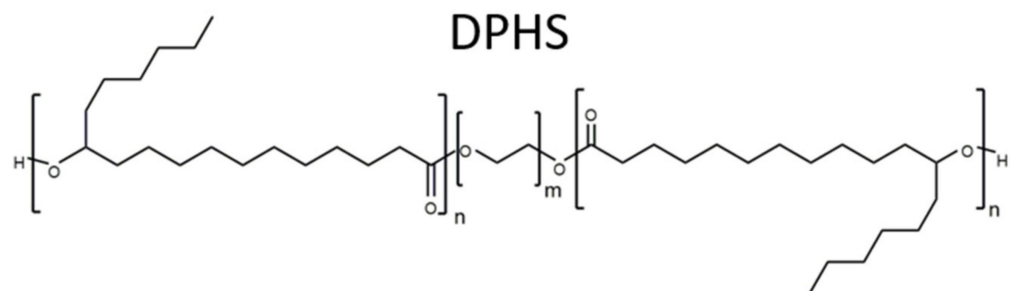


Figure 3. Chemical structure of Cithrol DPHS ($m = 30$, $n = 9$).

2.2. Preparation Methods

Bulk samples typically were a binary system which consisted of distilled water and a primary surfactant (PS). By the addition of oil, a ternary system was formed. Bulk samples had a typical total mass of (1000 ± 20) mg. The ingredients were weighed with an analytical balance ($\Delta m = \pm 0.1$ mg) and stored in 4 mL vials and heated up to a temperature of 80°C for 5 min in order to melt any occurring LC-phases before agitation with a vortex (RS-VA 10 by Phoenix Instrument, Garbsen, Germany) until room temperature was reached. The binary system water/surfactant is characterised by the mass ratio of the primary surfactant (PS)

$$\delta = \frac{m_{PS}}{m_{PS} + m_{H_2O}} \cdot 100 \quad (1)$$

Ternary systems were formed by adding defined amounts of oil (given in %_w of the total bulk mass) to the binary system. After vortexing, bulk samples with the PS Genapol were centrifuged for one hour at 4500 rpm (Labofuge 400R by Heraeus, Hanau, Germany) in order to remove entrapped air bubbles that had formed during vortexing. Samples with the primary surfactant P94 did not require this procedure due to the low-foaming characteristics of this surfactant. All bulk samples were equilibrated at room temperature for one day before any measurements were taken.

Dispersions consisted of the components of the ternary system along with an additional surfactant (stabiliser). The stabiliser was dissolved in the oil phase (0.5%_w-solution of Pickering stabiliser; 1%_w-solution of molecular stabiliser). An ultra-sonication device (Vibra-Cell by Sonics & Materials, Newtown, CT, USA) with a tapered tip was used at a power of 120 W in pulsed mode (0.3 s pulses with breaks of 2 s). The samples were placed in a water bath with additional ice to avoid over-heating of the components. As a first step, the PS was combined with the oil and the stabiliser-solution and dispersed for 2 min before the last component, distilled water, was added and the samples were again dispersed for 10 min. The dispersions can be characterised by the δ -value and two more variables related to the amount of stabiliser and the total concentration of ISAsomes in the dispersion:

$$\beta = \frac{m_{Stabiliser}}{m_{PS} + m_{H_2O}} \cdot 100 \quad (2)$$

$$\phi = \frac{m_{PS} + m_{H_2O}}{m_{PS} + m_{H_2O} + m_{Stabiliser} + m_{Oil}} \cdot 100 \quad (3)$$

Dispersion samples had a typical total mass of (2000 ± 50) mg and were stored in 4 mL vials. Unless specified otherwise, all dispersion samples were equilibrated at T_{RT} for 1 h before further characterisation with SAXS, dynamic light scattering (DLS) or polarisation light microscopy (PLM).

Polarisation light microscopy (PLM): A Leica DM2500 M microscope (Leica Camera AG, Wetzlar, Germany) with two polarisation filters was used for the determination of anisotropic samples (refer to chap. 2.4 for details). The samples were squeezed between two glass plates and investigated in transmittant light mode with various objective lenses. A Sony DXC-390P camera (Sony, Tokio, Japan) was mounted on the microscope and the pictures were recorded with the software Sarfusoftware 2.1 (Nanolane, Le Mans, France).

Dynamic light scattering (DLS): The mean hydrodynamic radius of the dispersion droplets was determined with dynamic light scattering (DLS). The equipment consisted of a Litesizer™ 500 (Anton Paar GmbH, Graz, Austria) that operates with a solid-state semiconductor laser diode with a wavelength of 658 nm at a power of 40 mW. The light scattering signal of each sample was measured five times for 1 min at a scattering angle of 90° and a temperature of 25°C . The data was analysed with the software Kalliope 2.20.2 by the application of the cumulant method [133]. An Abbat 550 refractometer and an MCR 502 rheometer (rotational mode) (both from Anton Paar GmbH, Graz, Austria) were used for the determination of the index of refraction and the viscosity of oils at 25°C .

Small-angle X-ray scattering (SAXS): A high flux SAXSess camera (Anton Paar GmbH, Graz, Austria) connected to a DebyeFlex 3003 X-ray generator (Ge-Electric, Frankfurt, Germany) with a sealed-tube Cu-anode was used. The operating settings of the generator were set to 40 kV and 50 mA which results in the X-ray wavelength $\lambda = 1.5420 \text{ \AA}$ (Cu-K- α radiation). A line-shaped X-ray beam (17 mm horizontal extension at the sample) was focused with a Goebel mirror and collimated with a Kratky slit. The scattered beam was measured in transmission mode with a 1D MYTHEN-1k microstrip solid state detector (Dectris AG, Baden, Switzerland) in a range of $q = (0.1\text{--}6) \text{ nm}^{-1}$, where q denotes the absolute value of the scattering vector defined as $q = \frac{4\pi}{\lambda} \cdot \sin\left(\frac{\theta}{2}\right)$ with the total scattering angle θ . In special cases where a higher resolution was needed, a SAXSpoint 2.0 system (Anton Paar GmbH, Graz, Austria) was used. The camera was connected to a Primux 100 micro X-ray source with an X-ray wavelength $\lambda = 1.5418 \text{ \AA}$ (Cu-K- α radiation) and a 2D Eiger detector was used. The measurements were taken in a range of $q = (0.0012\text{--}5.5) \text{ nm}^{-1}$, and the data acquisition and conversion were performed with the software packages SAXSdrive (version 2) and SAXSanalysis (version 4). Unless specified otherwise, all measurements were taken at a temperature of 20°C (T_{RT}).

3. Results

3.1. Investigations on Bulk Samples

As stated in the section “Materials and Methods”, binary bulk samples are formed by mixing the primary surfactant (PS) with water. A ternary bulk phase was formed by addition of oil to the binary mixture to test the ability of the hydrophilic LC-phases to coexist with excess amounts of oil. The bulk samples were investigated with SAXS measurements and, where necessary, polarisation light microscopy (PLM) was used to investigate the structure of the LC-phases. Binary bulk phases were typically clear, highly viscous liquid crystals. Microemulsions/ L_1 -phases typically appeared as transparent fluids. Upon the addition of excess oil, a turbid, inhomogeneous two-phase system (oil-saturated LC + excess oil) was obtained.

3.1.1. Genapol–Squalane System

The first system was based on the PS Genapol LA 070, a polyethylene glycol alkyl ether that has shown beneficial behaviour in past studies [130,134]. The SAXS curves of the binary system Genapol–water are shown in Figure 4. For surfactant concentrations $40 \leq \delta \leq 60$, a hexagonal phase (H_1) was formed that changed to a lamellar structure (L_α) for $\delta \geq 70$ (characterised by equidistant peak positions and the appearance of characteristic “maltese crosses” in the PLM image). The hexagonal phase was identified by the characteristic position of the SAXS-peaks ($q_0, \sqrt{3}q_0, 2q_0$) and the hexagonal lattice parameter can be calculated from the position of the primary peak q_0 [7]. The lattice parameter changed from (7.19 ± 0.05) nm ($\delta = 40$) to (6.21 ± 0.04) nm ($\delta = 60$) due to a decreased hydration of the hydrophilic headgroups at a lower water content. At lower surfactant concentrations ($\delta \leq 30$), the formation of an isotropic micellar solution (L_1) could be observed.

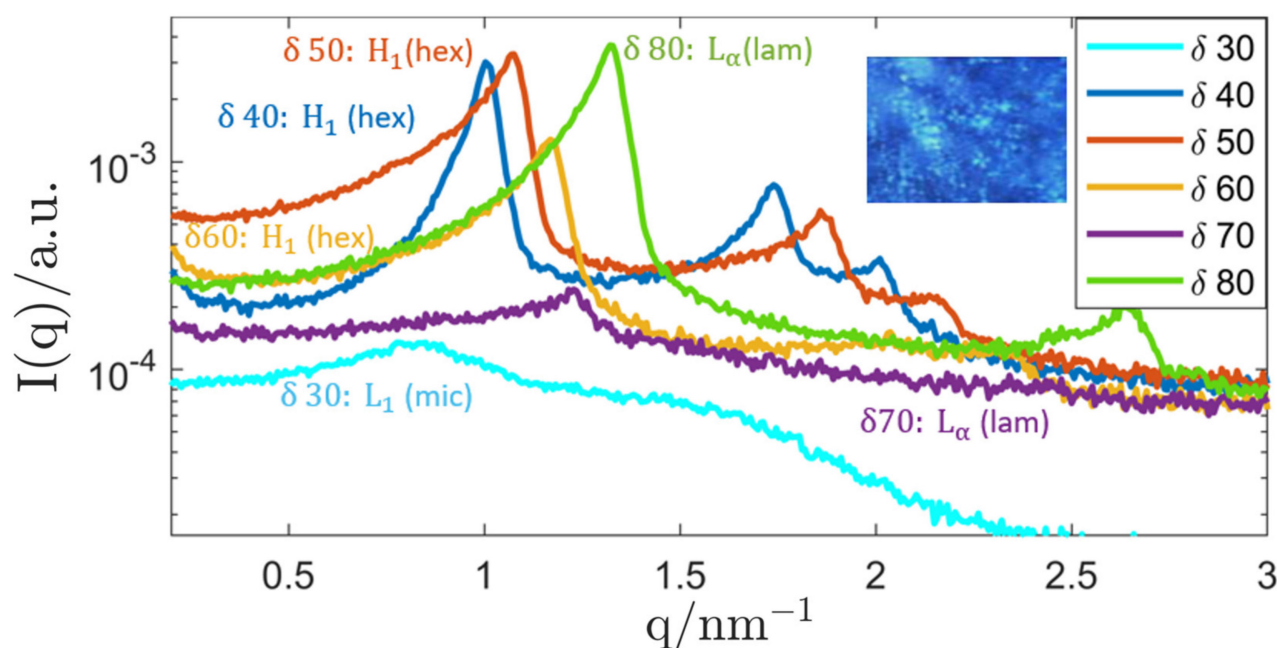


Figure 4. Selected SAXS measurements of samples with varying surfactant concentration δ in the range $\delta = (30\text{--}80)$. The hexagonal scattering curves are emphasised in the plot. For better readability, the curves are labelled with the assigned LC-phases H_1 ... hexagonal, L_α ... lamellar, L_1 ... isotropic micellar. The inset shows the PLM image (magnification 20) of a liquid-crystalline phase with $\delta = 70$ that is typical for lamellar anisotropy (maltese crosses weakly visible). All graphs were shifted by an arbitrary factor for better readability.

Based on those results, bulk samples at selected surfactant concentrations were loaded with increasing amounts of squalane to investigate its influence on the LC-structure and the possibility of full oil-saturation while maintaining the LC-phase. The corresponding SAXS measurements are shown in Figure 5.

At low surfactant concentrations δ , a microemulsion (swollen micellar solution) was formed by incorporation of squalane into the micellar aggregates. The corresponding SAXS curves show the broad correlation peak that corresponds to the mean centre-to-centre distance of the micelles.

As can be seen, the system saturated at an oil concentration of 15 %_w without deterioration of the structure. Therefore, the most important prerequisite for the dispersion of the system and the formation of an inverse emulsified microemulsion (EME) was given.

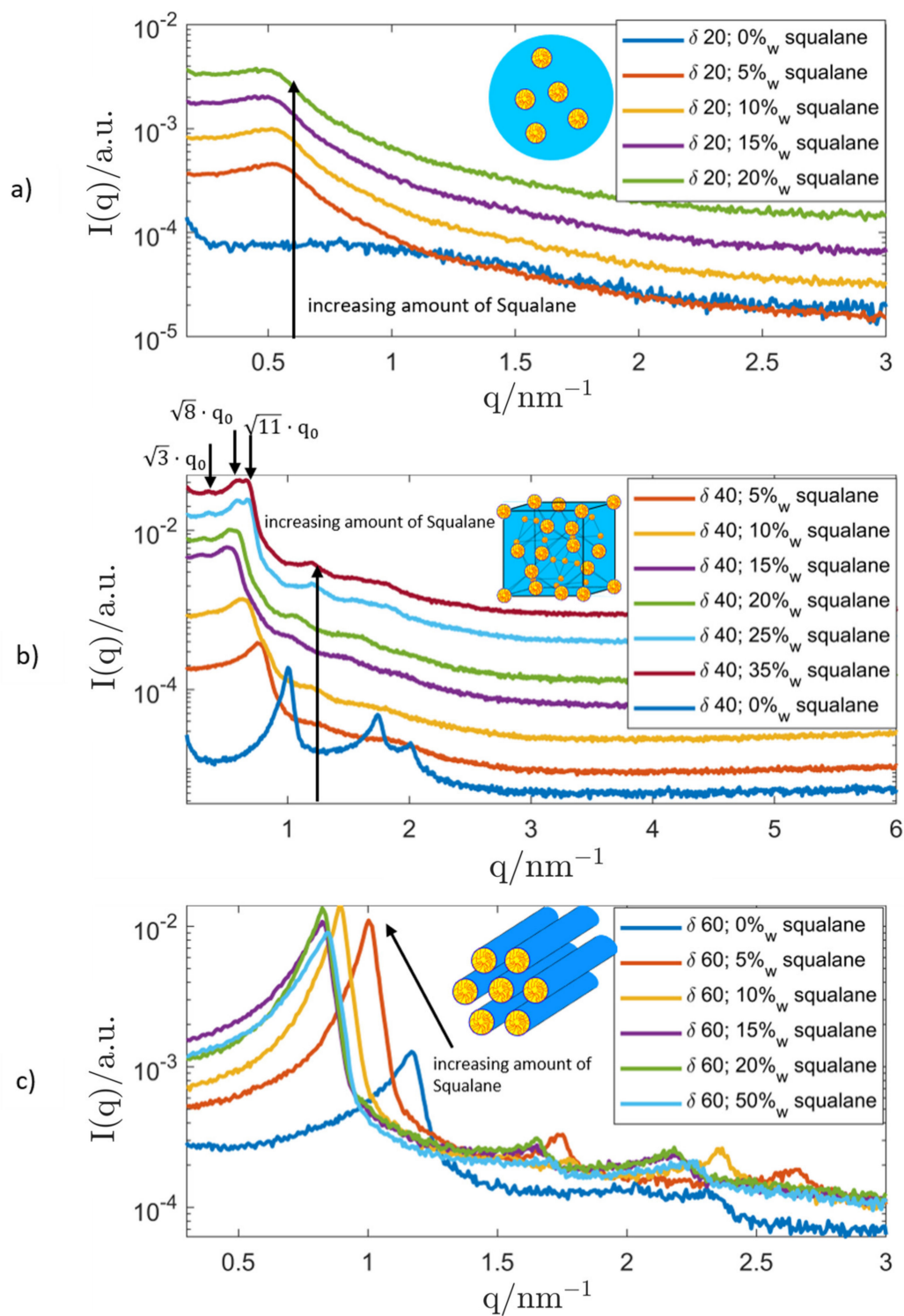


Figure 5. SAXS curves of samples with varying surfactant concentration: $\delta =$ (a) 20; (b) 40; (c) 60 and increasing amounts of squalane (given in %_w). The downward arrows in the middle panel show the position of the characteristic SAXS-peaks of the micellar cubic Fd3m phase. All graphs were shifted by an arbitrary factor for better readability. The insets show schematic depictions of the detected LC-phases: Top: microemulsion; Middle: micellar cubic (I_1 , Fd3m); Bottom: hexagonal (H_1).

Based on the behaviour of the binary system Genapol/water, the oil-loading of a hexagonal structure was attempted. However, upon incorporation of squalane into its structure, bulk samples with a surfactant concentration $\delta = 40$ showed a radical change in phase behaviour, as revealed by the SAXS measurement: The initial hexagonal phase started to change upon addition of small amounts of squalane. At higher oil concentrations ($\geq 10\%_w$), a micellar cubic phase (I_1) with Fd3m symmetry started to develop. The structure of this LC-phase was first described by Mariani et al. [135]. As expected, the peaks shifted towards smaller q -values with increasing concentration of squalane which signifies a swelling of the structure, as more and more oil was incorporated into the micelles. When the oil concentration was increased even further, a micellar cubic phase with Fd3m symmetry started to coexist with the microemulsion until the pure, oil-saturated Fd3m-phase was found at an oil concentration of $25\%_w$ and a lattice parameter of (31.1 ± 0.2) nm. Investigations with the polarised light microscope (PLM) showed no signs of anisotropy, which supported the existence of a cubic LC-phase. As the system could coexist with excess amounts of oil, the prerequisite for the dispersion and creation of inverse micellar cubosomes was given.

At even higher values of the surfactant concentration ($\delta = 60$), the expected swelling of the hexagonal structure could be observed. The hexagonal LC-phase remained stable, and the lattice parameter of the binary mixture (6.21 ± 0.04) nm started to swell until saturation was reached at a squalane concentration of $13.2\%_w$ and a lattice parameter of (8.81 ± 0.07) nm, as shown in Figure 6.

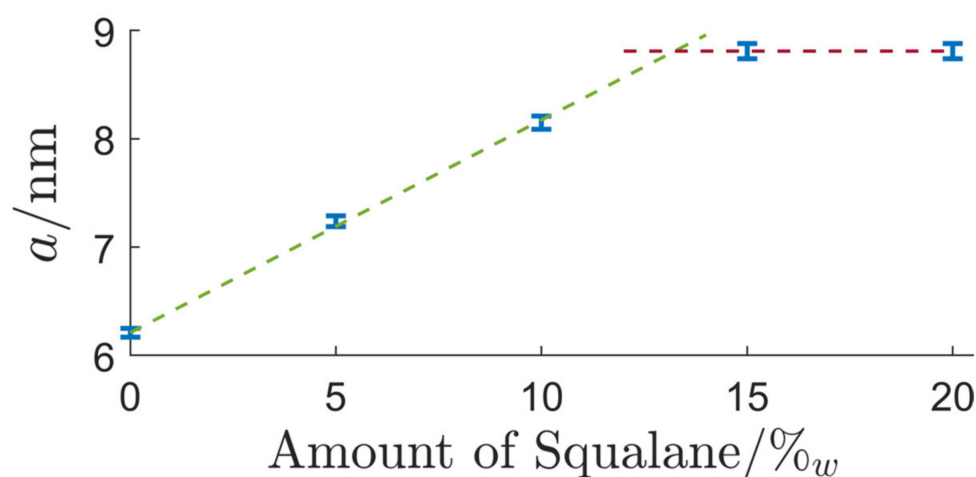




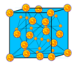
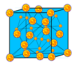
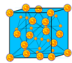

Figure 6. Depiction of the growing lattice parameter a of the hexagonal phase with addition of increasing amounts of squalane. A linear fit was applied to the growth region and the saturated regime to determine the saturation oil concentration.

An overview of binary bulk phases observed at the surfactant concentrations $\delta = 20, 40, 60$ along with the corresponding, oil-saturated systems is given in Table 1.

As in the cases before, the stability of the hexagonal phase upon saturation with squalane was the most important prerequisite for the dispersion of the hydrophilic LC and the formation of inverse hexosomes.

The combination of the binary system Genapol/H₂O with triolein as the excess oil phase showed no promising results in experiments. The addition of triolein greatly influenced the stability of the LC-phases and only less well-defined mixed-phase configurations could be achieved in the ternary system. Therefore, this system configuration was omitted for the production of inverse ISAsomes and an alternative primary surfactant, P94, was ultimately used in combination with triolein.

Table 1. Overview of the LC-phases observed in bulk samples in the system Genapol/squalane (Gena/Squal). Samples with selected surfactant concentrations $\delta = 20, 40, 60$ are shown. The corresponding oil-saturated systems with the observed LC-phases are also shown. The lattice parameter a , where applicable, is also displayed. The sketches of the LC-phases correspond to the structure that was observed in the oil-saturated samples at each value of δ .

System Composition	δ	LC-Phase		a/nm
Gena	20	L_1		n.a.
Gena+Squal _{20%}	20	L_1		n.a.
Gena	40	H_1		7.19
Gena+Squal _{25%}	40	I_1		31.1
Gena	60	H_1		6.21
Gena+Squal _{20%}	60	H_1		8.81

3.1.2. P94/Triolein System

In analogy to the Genapol-system, binary bulk samples with different ratios of water/P94 were produced. Selected SAXS curves are presented in Figure 7. The results were compared with a known phase diagram from another contribution [13], and for the most part, no discrepancies with literature could be identified. Starting at a surfactant concentration of $\delta = 30$, a micellar solution (L_1) was formed. However, the cubic phase (I_1) predicted by the phase diagram at a surfactant concentration of $\delta = 37$ could not be confirmed with SAXS measurements. The SAXS curve showed some unidentified type of order that could signify a mixed-phase system of H_1 and another phase with unidentified order. As no pure, non-mixed LC-structure could be confirmed with SAXS measurements, samples with this composition were omitted for the production of inverse ISAsomes. When raising the surfactant concentration to $\delta = 50$, the expected hexagonal (H_1) phase was formed and maintained a lattice parameter of (10.93 ± 0.11) nm until it changed to a mixed-phase system ($H_1 + L_\alpha$) at $\delta = 70$ and to a lamellar structure at even higher values of δ .

Again, samples at selected surfactant concentrations were loaded with increasing amounts of oil and the robustness of the LC-phases was verified with SAXS (shown in Figure 8). Triolein was chosen as the oil phase as it is a triglyceride with a well-defined molecular structure that can be used as a model oil for commercially available food-grade oils (e.g., olive oil). It is necessary to mention at this point that polarisation light microscopy (PLM) was hardly applicable in this system due to a low birefringence of the H_1 and L_α phases formed by the primary surfactant P94.

At a surfactant concentration of $\delta = 30$, the addition of triolein to the binary micellar solution showed no measurable effect on the micellar structure, as can be seen in Figure 8. The broad SAXS correlation peak (starting at $q = 1.5 \text{ nm}^{-1}$) is characteristic for samples that contain a triglyceride and can be attributed to the molecular order in these oils [136]. It can be deduced, that micelles formed by the primary surfactant P94 incorporate hardly any triolein. Due to the robustness of the micellar structure against addition of excess amounts of triolein, the decision was made to attempt a dispersion of this system.

A surfactant concentration of $\delta = 55$ was chosen for oil-loading of the hexagonal structure: As for the other two structures, the hexagonal lattice seemed to incorporate hardly any oil and the prerequisite for the dispersion of the system in excess triolein was given. The oil compatibility of hydrophilic LC-phases formed by the primary surfactant P94 was also tested with squalane where a similar result was obtained. As hardly any oil is incorporated into the LC-structures, the ability to coexist with a large variety of oils could be given. An overview of binary bulk phases observed at the surfactant concentrations $\delta = 30$ and 55 along with the corresponding, oil-saturated systems is given in Table 2.

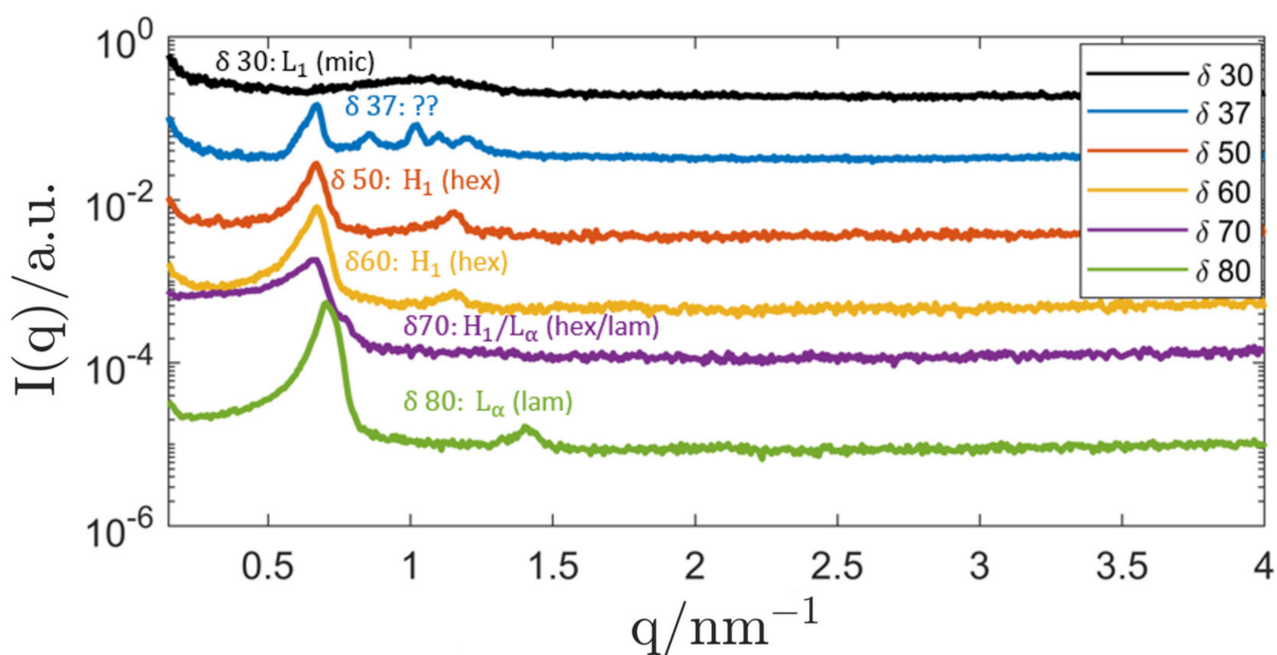


Figure 7. SAXS curves of the binary system P94/H₂O with varying surfactant concentration δ . For better readability, the curves are labelled with the assigned LC-phases: L_1 ... isotropic micellar solution, H_1 ... hexagonal, L_α ... lamellar, H_1/L_α ... two-phase mixture hexagonal/lamellar. The hexagonal scattering curves are emphasised in the plot. The sample with $\delta = 37$ was equilibrated at a temperature of 5 °C for 1 day and at T_{RT} for another day. The measurements of samples with $\delta \leq 37$ were performed with the SAXS camera “SAXSpoint 2.0” for better resolution. All curves were shifted by an arbitrary factor for better readability.

Table 2. Overview of the LC-phases observed in bulk samples in the system P94/Triolein. Samples with selected surfactant concentrations $\delta = 30$ and 55 are shown. The corresponding oil-saturated systems with the observed LC-phases are also shown. The lattice parameter a of the hexagonal phase is also displayed. The sketches of the LC-phases correspond to the structure that was observed in the oil-saturated samples at each value of δ .

System Composition	δ	LC-Phase	a/nm
P94	30	L_1	n.a.
P94+Triolein _{5%}	30	L_1	n.a.
P94	55	H_1	10.93
P94+Triolein _{20%}	55	H_1	10.93

3.2. Dispersion and Stabilisation

As both systems, Genapol/H₂O/squalane and P94/H₂O/triolein showed capabilities to form stable hydrophilic LC-phases in the presence of excess amounts of oil, the dispersion and stabilisation of both systems was attempted. The creation of dispersion samples is described in the section “Materials and Methods”. ISAsome dispersions typically appear as a turbid medium with white colour. Samples in excess squalane had a white colour, while samples dispersed in triolein and olive oil appeared as yellow, milk-like liquid.

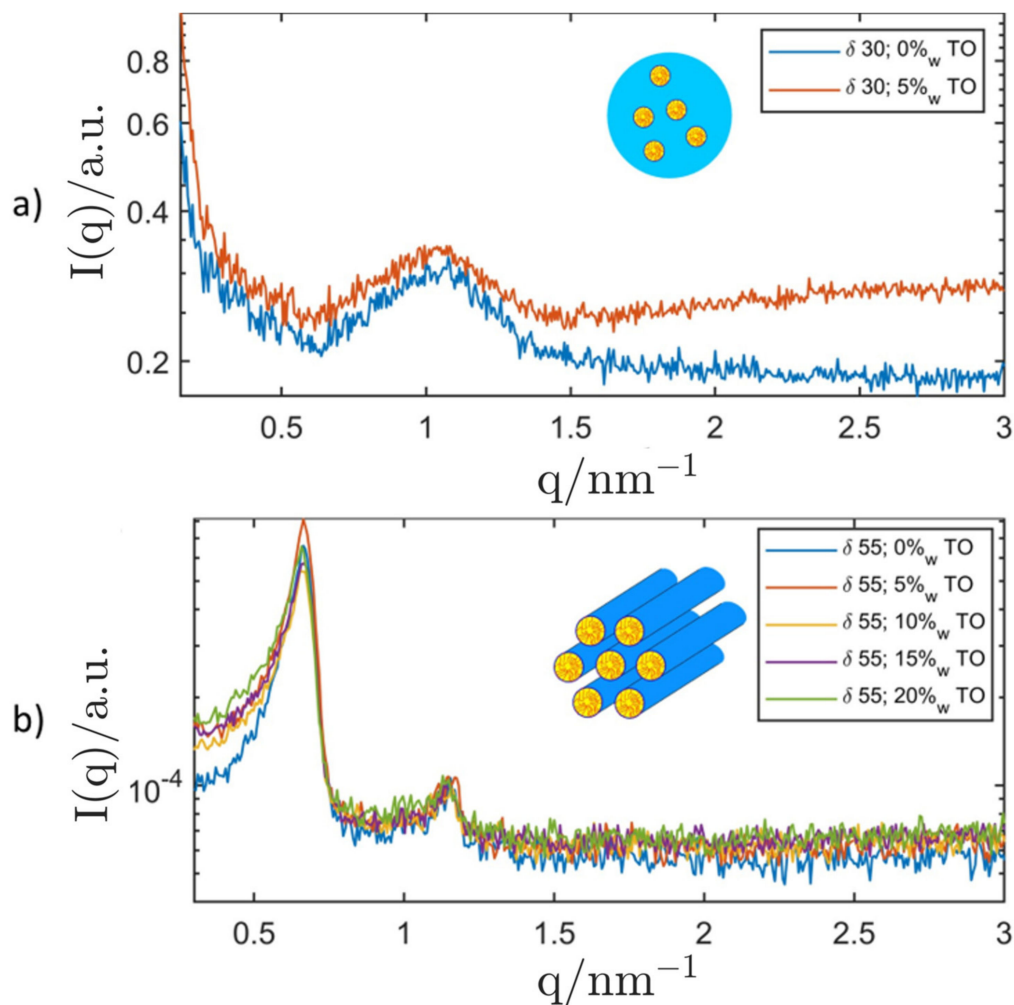


Figure 8. SAXS curves of the ternary system P94/H₂O/TO at different surfactant concentrations ($\delta =$ (a) 30 & (b) 55) with added triolein (TO) and the corresponding binary systems without added oil. The measurements for the samples with $\delta = 30$ were performed with the SAXS camera "SAXSpoint 2.0" for better resolution. The insets show schematic depictions of detected LC-phases. Top: micellar isotropic L_1 -phase; Bottom: hexagonal H_1 -phase.

3.2.1. Genapol/Squalane System

A variety of stabilisers was tried for dispersed LC-phases of this system. Stabilisation attempts with polymeric stabilisers (e.g., DPHS and reverse Pluronics) were not fruitful and all dispersion samples showed aggregation and phase separation rather quickly.

The final stabilisation attempt was performed with R711-nanoparticles. The impact of a varying surfactant concentration δ at a fixed stabiliser concentration β and a fixed ISAsome concentration ϕ was investigated. The results are displayed in Figure 9. In analogy to previous works [130], the primary hexagonal peak could be clearly measured in this Pickering emulsion, while higher-order peaks were often hard to detect due to the background scattering intensity of the silica nanoparticles. The presence of the hexagonal phase ($\delta = 70$) was confirmed with the help of the PLM that showed clear signs of non-lamellar anisotropy. The hexagonal lattice parameter was determined as (8.28 ± 0.07) nm, which was slightly lower than the value measured in the oil-saturated bulk phase. This phenomenon could be attributed to an interaction of the stabiliser with the LC-phase, where parts of the primary surfactant were adsorbed at the silica nanoparticles until they were saturated [130]. This also led to a shift of the surfactant concentration δ between bulk samples and corresponding dispersion that could be observed for all structures. Inverse hexosomes, e.g., were found at $\delta = 70$ while corresponding, oil-saturated hexagonal bulk

samples were only found at a lower surfactant concentration ($\delta = 60$). Nevertheless, the production of Pickering-stabilised inverse hexosomes in excess squalane was successful.

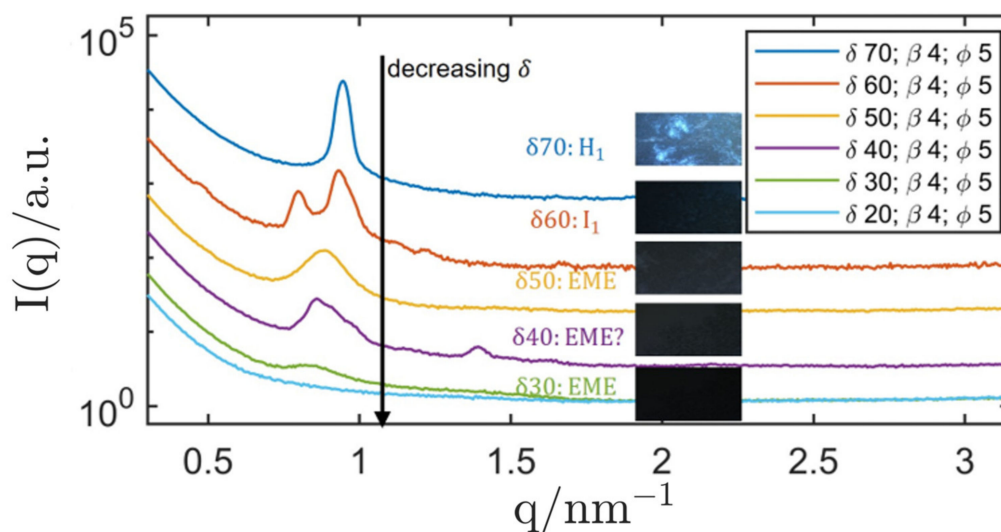


Figure 9. SAXS curves of R711 Pickering emulsions (Genapol/H₂O in squalane) with $\beta = 4$ and varying surfactant concentration δ . The inset shows the respective PLM images. The sample with $\delta = 60$ was heated to 37 °C before measuring at 20 °C to obtain the Fd3m structure. In order to improve the quality of the measurement data of this sample, a scan of the empty capillary was taken and subtracted. For better readability, the curves are labelled with the assigned LC-phases: H_1 . . . hexagonal, EME . . . emulsified microemulsion I_1 . . . micellar cubic (Fd3m symmetry). The SAXS curves of all samples were measured with the SAXS camera “SAXSpoint 2.0” for better resolution. All graphs were shifted by an arbitrary factor for better readability.

The characterisation of the dispersion with $\delta = 60$ with SAXS revealed the existence of a micellar cubic phase with Fd3m symmetry. The structure only developed after heating the sample to 37 °C before finally taking the measurement at 20 °C, which could signify that the thermodynamical equilibrium of the LC-phase is only reached after applying this heating scheme. It might be related to the fact that samples were cooled in an ice bath during dispersion. After the described heating, the samples maintained their Fd3m structure when they were being stored at a temperature of 20 °C. A cooling of the sample to 5 °C induced a change to an inverse emulsified microemulsion (EME).

As can be seen in Figure 10, the micellar cubosome structure was clearly shifted with respect to the oil-saturated bulk phase. While the latter had a lattice parameter of (31.1 ± 0.2) nm, the cubosomes showed a smaller lattice parameter of (22.3 ± 0.2) nm. As mentioned above, the stabilisation of the cubosomes with silica nanoparticles might lead to a significant decrease in the effective surfactant concentration δ (also hinted at by the relatively large shift of δ when compared to the oil-saturated bulk-phase). SAXS measurements clearly showed the micellar cubic structure of the dispersion, and the PLM showed no signs of anisotropy. Therefore, the development of Pickering-stabilised inverse micellar cubosomes (Fd3m symmetry) was successful.

When the surfactant concentration δ was chosen below 60, the structure gradually changed to an inverse emulsified microemulsions (EME) and a dispersion with $\delta = 40$ showed signs of a mixed-phase system, signified by the appearance of a second peak and a disturbed primary peak. At $\delta = 30$, the SAXS measurement showed clear signs of an inverse emulsified microemulsion (EME). The dispersion was compared with SAXS measurements of oil-saturated bulk samples (microemulsions) and the results are shown in Figure 11.

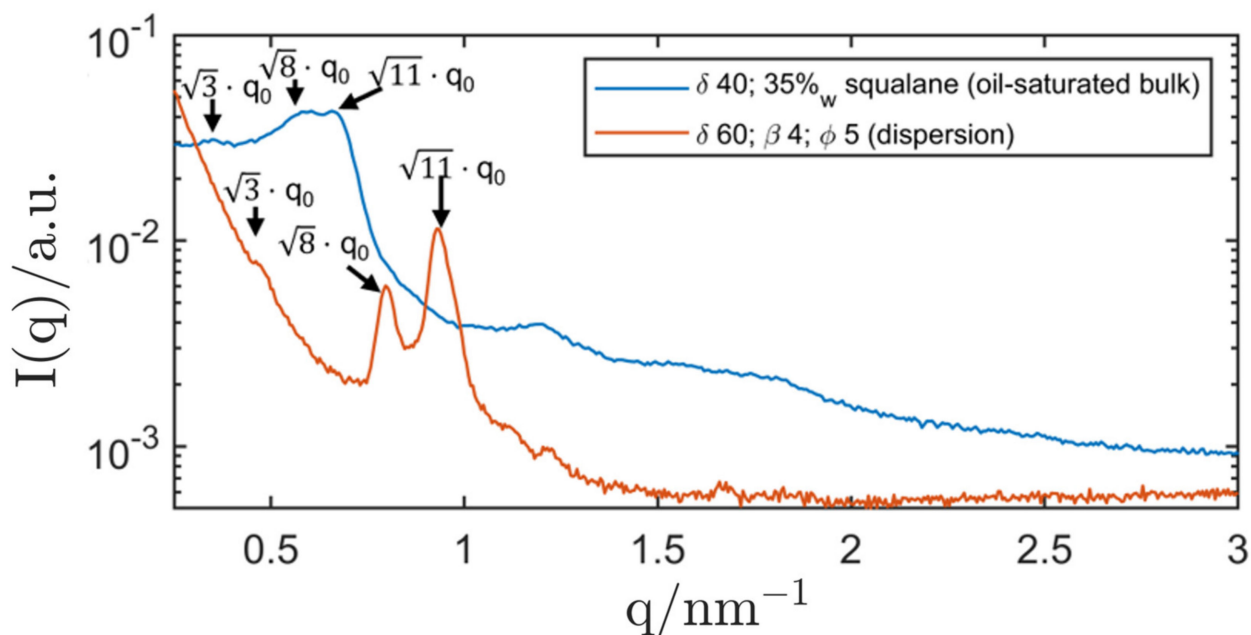


Figure 10. SAXS curves of R711 Pickering emulsions (Genapol/H₂O in squalane) with a contained micellar cubic phase (Fd3m symmetry) and arrows signifying the position of the characteristic SAXS peaks of this phase. The dispersion was heated to 37 °C before measuring at 20 °C to obtain the Fd3m structure. For comparison, the corresponding oil-saturated bulk phases is also displayed. In order to improve the quality of the measurement data of the dispersion, a scan of the empty capillary was taken and subtracted. The SAXS curve of the dispersion was measured with the SAXS camera “SAXSpoint 2.0” for better resolution.

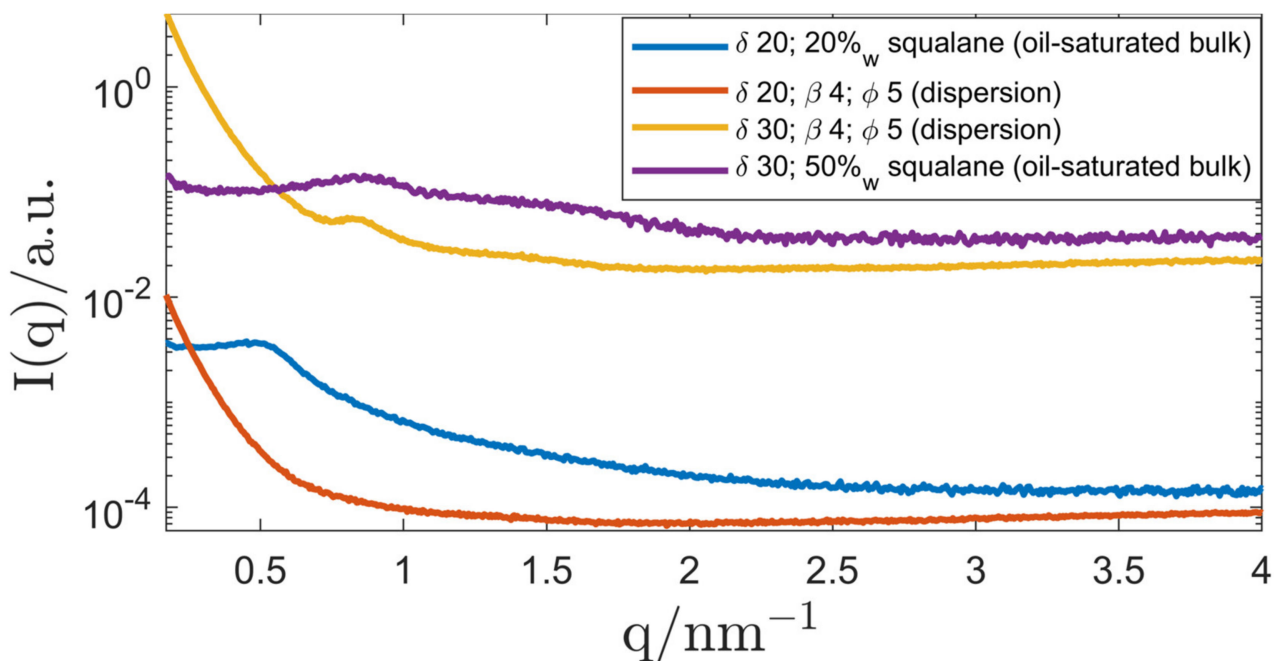


Figure 11. SAXS curves of R711 Pickering emulsions (Genapol/H₂O in squalane) with $\delta = (20-30)$. For comparison, the corresponding oil-saturated bulk phases are also displayed. The SAXS curves of the dispersions were measured with the SAXS camera “SAXSpoint 2.0” for better resolution. All graphs were shifted by an arbitrary factor for better readability.

At a surfactant concentration of $\delta = 30$, the peak position of the bulk sample (oil-saturated microemulsion) was in accordance with that of the corresponding dispersion. Therefore, the existence of an inverse emulsified microemulsion (EME) could be shown. When lowering δ to 20, the correlation peak of the EME could not be measured with SAXS anymore.

All Pickering emulsions showed aggregation nearly immediately which prevented the characterisation of the particle size with DLS. The aggregate size was measured with the polarisation light microscope (PLM) and was estimated to be in a range of (100–300) μm . No phase separation was observed in a time span of one month.

3.2.2. P94/Triolein System

Based on knowledge gained from previous studies [132], DPHS was chosen for the steric stabilisation of inverse ISAsomes in triolein. Again, the surfactant concentration δ was varied and the appearing structures were characterised with SAXS. In addition, triolein was ultimately exchanged with commercially available olive oil and the effect on the inverse ISAsomes was observed. The broad SAXS correlation peak typically shown by triglycerides often covered the signal from the structure of dispersed LC-phases which sometimes led to the necessity of further data processing to reveal structures.

At a surfactant concentration of $\delta = 60$, inverse hexosomes with a lattice parameter of (11.75 ± 0.12) nm were formed in triolein. The stabilisation with DPHS led to a typical hydrodynamic diameter in the sub- μm regime (measured with DLS) and no phase separation could be observed over the course of a month. The DLS data for the inverse hexosomes can be found in Table 3. When the stabiliser was omitted ($\beta = 0$), inverse hexosomes with an identical lattice parameter were formed and the dispersion showed surprisingly good steric stability. Aggregates with a size of (100–300) μm (measured with PLM) were formed and no phase separation could be observed. The stabilisation was most likely achieved by the long polymeric chains of the primary surfactant (P94) that ensure a minimum steric effect. When triolein was exchanged with commercially available olive oil, the inverse hexosomes were found to have a lattice parameter of (11.39 ± 0.10) nm which is slightly smaller than the value measured for the analogous system in triolein. It is probable that surface-active impurities in the olive oil are responsible for this small change of the lattice parameter. Stabilisation with DPHS showed mediocre results: The inverse hexosomes had a typical diameter of (50–100) μm (measured with PLM). The self-stabilising system without DPHS showed typical aggregate sizes of (100–300) μm (measured with PLM). The resulting SAXS curves of the inverse hexosomes are shown in Figure 12. The ISAsome concentration for the self-stabilising hexosomes in olive oil was lowered to $\phi = 5$ to achieve a better dispersion quality.

Table 3. DLS results for inverse ISAsomes dispersed in triolein and olive oil at various surfactant concentrations δ with a fixed stabiliser concentration $\beta = 5$ and a fixed ISAsome concentration $\phi = 10$. The mean diameter d as well as the polydispersity index (*PDI*) are shown.

Oil Phase	δ	d/nm	<i>PDI</i>
Triolein	30	216	23%
Triolein	60	134	23%
Olive oil	30	175	37%

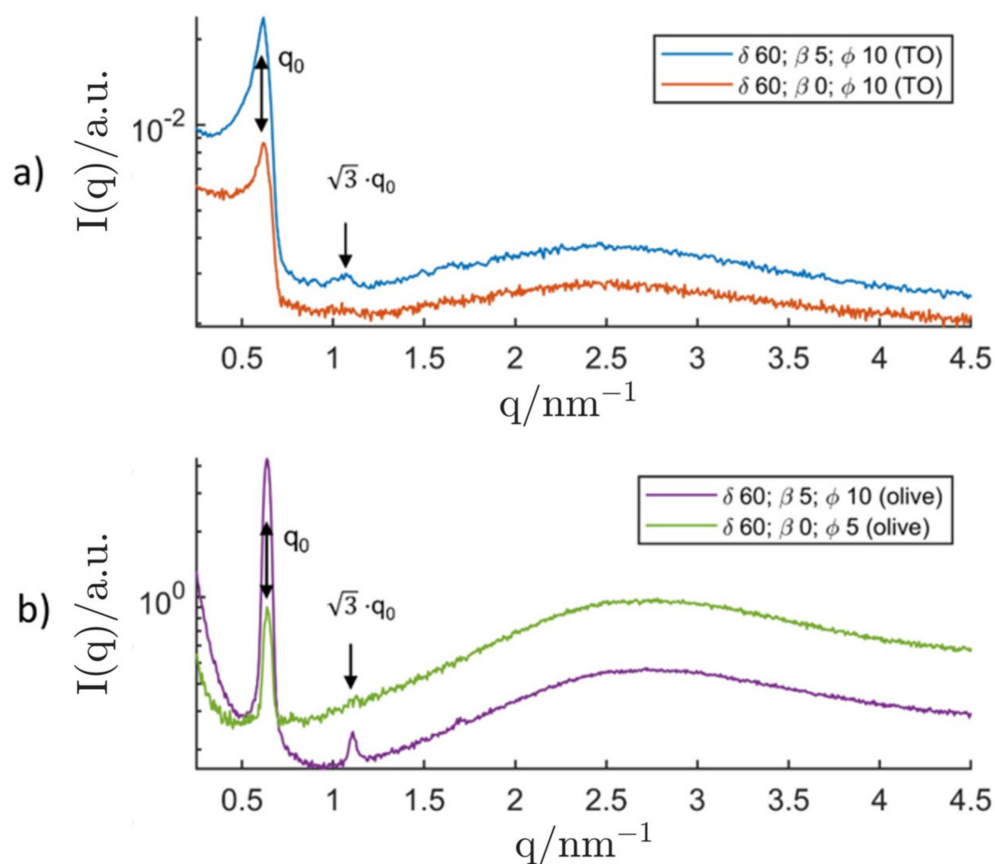


Figure 12. SAXS curves of successfully produced inverse hexosomes made of P94/H₂O. The upper graph (a) shows the hexosomes in triolein (TO) with ($\beta = 5$) and without ($\beta = 0$) additional stabiliser DPHS and a constant ISAsome concentration $\phi = 10$. At the bottom (b), the analogous system in olive oil is displayed. The SAXS curves of the bottom graph were measured with the SAXS camera “SAXSpoint 2.0” for better resolution. All graphs were shifted by an arbitrary factor for better readability.

For dispersions with a lower surfactant concentration of $\delta = 30$, SAXS curves showed a correlation shoulder at a position that is in accordance with the correlation peak of the oil-saturated bulk sample, as shown in Figure 13, and DLS measurements revealed a hydrodynamic diameter below 300 nm as shown in Table 3. As discussed above, micelles made of P94/H₂O do not incorporate measurable amounts of oil, which makes the categorisation of the (emulsified) bulk phase as “(emulsified) inverse microemulsion” questionable. In lack of an existing nomenclature, we decided to name the dispersed system as “emulsified L_1 -phase”.

SAXS measurements of the corresponding system in olive oil did not reveal the existence of an inverse EME or an emulsified L_1 -phase. It is possible that the micellar structure is somewhat disturbed by impurities of the olive oil. However, as shown in Table 3, DLS-measurements showed particle sizes comparable to those found in the triolein-system which could be an indication for the formation of a comparable system even though it could not be confirmed by SAXS.

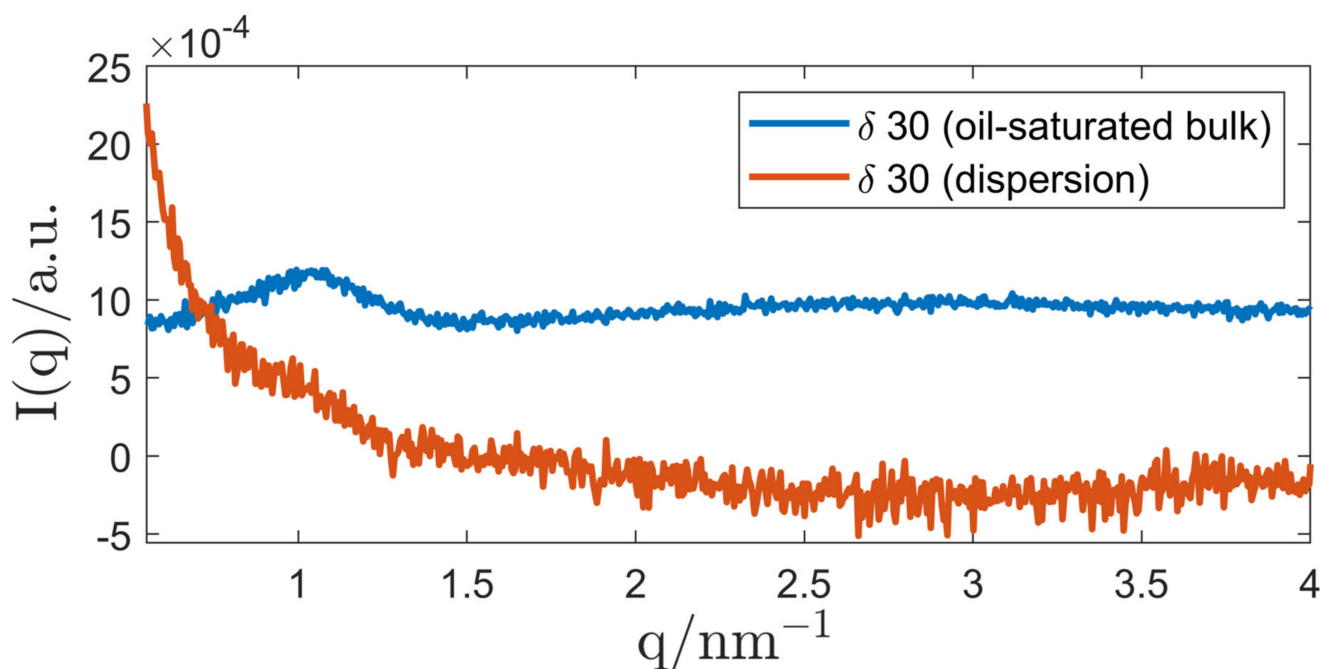


Figure 13. SAXS curves of an inverse EME made of P94/H₂O in TO. For comparison, the oil-saturated bulk phase is also displayed. All graphs were shifted by an arbitrary factor for better readability. A scattering curve of pure TO was subtracted from the dispersion curve to reveal the correlation shoulder of the emulsified L_1 -phase. The measurements were performed with the SAXS camera “SAXSpoint 2.0” for better resolution.

4. Discussion

In this contribution, we have shown the successful production of various types of inverse ISAsomes in two different systems. The first system used squalane as oil matrix and hydrophilic lyotropic LCs made of Genapol LA 070 (primary surfactant) and H₂O were dispersed and stabilised with the help of hydrophobised silica nanoparticles (Pickering stabilisation). Apart from inverse hexosomes, inverse micellar cubosomes and an inverse emulsified microemulsion (EME) were also found at different concentrations of the primary surfactant. To the best of our knowledge, this is the first report on the two latter types of inverse ISAsomes. The confined hydrophilic structures showed the capability to incorporate finite amounts of oil until saturation without deteriorating. The Pickering-stabilised dispersion droplets showed fast aggregation (aggregate size of (100–300) μm) but no phase separation could be observed in a time span of one month. Similar to previous contributions [130], the interaction of the stabiliser led to a decrease in the effective surfactant concentration δ . The primary surfactant tends to adsorb to the stabiliser until saturation is reached which requires larger amounts of the primary surfactant to achieve the structures that were previously observed in oil-saturated bulk samples. Stabilisation attempts with molecular stabilisers were not successful, and the future replacement of the silica nanoparticles with a food-grade stabiliser could enable a wider range of possible applications.

The second system used triolein as the oil-continuous phase. Particles made of P94 (primary surfactant) and H₂O were dispersed and stabilised with the molecular stabiliser Cithrol DPHS. Inverse hexosomes and an emulsified L_1 -phase were found. In contrast to an inverse EME, no oil is incorporated into its micellar nanostructure. The droplet size was in the range of (100–300) nm and no signs of phase separation could be found over the course of a month. In addition, stabiliser-free inverse hexosomes with aggregate sizes of (100–300) μm were produced. Most likely, the long polymeric chains of the primary surfactant lead to a steric stabilising effect that is sufficiently strong to prevent phase separation. The particles were named “self-stabilising inverse hexosomes” and could be

beneficial in, e.g., skin care applications where the presence of a large amount of surfactant molecules is often undesired. In all cases, lyotropic LC structures made of P94/H₂O incorporated hardly any triolein, a result that could also be replicated with other types of oil. As triolein is a highly pure model oil for natural plant oil, the replacement of triolein with commercially available olive oil was attempted. This resulted in the successful production of inverse hexosomes, both sterically stabilised and self-stabilising ones, with droplet sizes comparable to the twin system in triolein. To the best of our knowledge, this is the first report on inverse hexosomes formulated with a commercially available plant oil. The tendency of the binary system P94/H₂O to incorporate hardly any oil into lyotropic LC structures might be a hint at its capability to form inverse ISAsomes in a large variety of oils as the LC structures are mostly undisturbed by the presence of the oil phase.

When compared to “conventional” ISAsomes, inverse ISAsomes are a rather new field of research. The development of such systems in a variety of biocompatible oils could lead to many applications in the fields of pharmaceutical and food industry. Ointments or other oil-continuous substances could be formulated to contain inverse ISAsomes to enable the controlled release of medical agents after being absorbed by the skin. The self-stabilising system presented in this contribution could be of special interest here due to the absence of a stabilising secondary surfactant. In addition, inverse ISAsomes could be used for the encapsulation of nutrients and enrichment of food oils. Combined with the ability to build in a controllable release trigger for these nutrients, the nutritional value of various oils could be enhanced. The presented formulations in triolein and olive oil are a first step towards the formulation of fully food-grade inverse ISAsomes. In addition to the replacement of the highly pure model oil triolein with a larger variety of natural food oils, future research could focus on the optimisation of the other ingredients. As many poloxamers such as P94 are approved as food additives, future studies could focus on the replacement of the molecular stabiliser with a suitable molecular or Pickering stabiliser. Various other possibilities such as the incorporation of active molecules (e.g., enzymes) into the inverse ISAsomes could be explored and the formulation of bicontinuous inverse cubosomes remains untackled up to this day.

5. Conclusions

We have achieved, for the first time, the production of various types of inverse ISAsomes in bio-compatible oils. This contribution adds inverse micellar cubosomes with Fd3m symmetry, an inverse emulsified microemulsion, an emulsified *L*₁-phase and self-stabilising inverse hexosomes to the ISAsome family. While formulations in excess squalane showed various kinds of LC-nanostructures, the successful production of inverse ISAsomes in the food-grade oil phases triolein and olive oil might be an especially interesting starting point for studies that could explore a fully food-grade system for the oral delivery of various kinds of nutrients. As the field of research on inverse ISAsomes is rather unexplored when compared to the well-established “conventional” ISAsome dispersions in aqueous solutions, we believe that this contribution can be a starting point for opening up new pathways for both, basic research and applications. Further studies of the given systems could include their characterisation with Cryo-TEM and other experimental techniques that were not within the scope of this project.

Author Contributions: Conceptualization, A.C. and O.G.; methodology, A.C. and O.G.; formal analysis, F.T.; investigation, F.T.; resources, A.C.; data curation, F.T.; writing—original draft preparation, F.T.; writing—review and editing, F.T., A.C. and O.G.; visualization, F.T.; supervision, A.C. and O.G.; project administration, A.C. and O.G. All authors have read and agreed to the published version of the manuscript.

Funding: Open Access Funding by the Graz University of Technology.

Institutional Review Board Statement: Not applicable.

Informed Consent Statement: Not applicable.

Data Availability Statement: Measurement data available upon request to the corresponding author.

Acknowledgments: The authors are especially thankful to Frank Uhlig for supporting the realisation of this project at his institute. Many thanks go to Stefan Salentinig and Wolfgang Sprengel for supporting the project and the master's thesis linked to it. The authors would like to acknowledge use of the Somapp Lab, a core facility supported by the Austrian Federal Ministry of Education, Science and Research, the Graz University of Technology, the University of Graz and Anton Paar GmbH. We would also like to acknowledge that the publication of this contribution was supported by the TU Graz Open Access Publishing Fund.

Conflicts of Interest: The authors declare no conflict of interest.

References

1. Huibers, P.D.T.; Lobanov, V.S.; Katritzky, A.R.; Shah, D.O.; Karelson, M. Prediction of Critical Micelle Concentration Using a Quantitative Structure–Property Relationship Approach. 1. Nonionic Surfactants. *Langmuir* **1996**, *12*, 1462–1470. [[CrossRef](#)]
2. Swope, W.C.; Johnston, M.; Duff, A.I.; McDonagh, J.; Anderson, R.L.; Alva, G.; Tek, A.T.; Maschino, A.P. Challenge to Reconcile Experimental Micellar Properties of the CnEm Nonionic Surfactant Family. *J. Phys. Chem. B* **2019**, *123*, 1696–1707. [[CrossRef](#)] [[PubMed](#)]
3. Vishnyakov, A.; Lee, M.-T.; Neimark, A.V. Prediction of the Critical Micelle Concentration of Nonionic Surfactants by Dissipative Particle Dynamics Simulations. *J. Phys. Chem. Lett.* **2013**, *4*, 797–802. [[CrossRef](#)] [[PubMed](#)]
4. Phillips, J.N. The energetics of micelle formation. *Trans. Faraday Soc.* **1955**, *51*, 561–569. [[CrossRef](#)]
5. Larsson, K. On the structure of isotropic phases in lipid-water systems. *Chem. Phys. Lipids* **1972**, *9*, 181–195. [[CrossRef](#)]
6. Dave, N.; Joshi, T. A Concise Review on Surfactants and Its Significance. *Int. J. Appl. Chem.* **2017**, *13*, 663–672.
7. Kulkarni, C.V.; Wachter, W.; Iglesias-Salto, G.; Engelskirchen, S.; Ahualli, S. Monoolein: A magic lipid? *Phys. Chem. Chem. Phys.* **2011**, *13*, 3004–3021. [[CrossRef](#)]
8. Shao, X.; Bor, G.; Al-Hosayni, S.; Salentinig, S.; Yaghmur, A. Structural characterization of self-assemblies of new omega-3 lipids: Docosahexaenoic acid and docosapentaenoic acid monoglycerides. *Phys. Chem. Chem. Phys.* **2018**, *20*, 23928–23941. [[CrossRef](#)]
9. Pfrang, C.; Rastogi, K.; Cabrera-Martinez, E.R.; Seddon, A.; Dicko, C.; Labrador, A.; Plivelic, T.S.; Cowieson, N.; Squires, A.M. Complex three-dimensional self-assembly in proxies for atmospheric aerosols. *Nat. Commun.* **2017**, *8*, 1724. [[CrossRef](#)]
10. Li, J.; Wang, X.; Zhang, T.; Wang, C.; Huang, Z.; Luo, X.; Deng, Y. A review on phospholipids and their main applications in drug delivery systems. *Asian J. Pharm. Sci.* **2015**, *10*, 81–98. [[CrossRef](#)]
11. Alexandridis, P.; Olsson, U.; Lindman, B. Self-Assembly of Amphiphilic Block Copolymers: The (EO)₁₃(PO)₃₀(EO)₁₃-Water-p-Xylene System. *Macromolecules* **1995**, *28*, 7700–7710. [[CrossRef](#)]
12. Khimani, M.; Patel, H.; Patel, V.I.; Parekh, P.; Vekariya, R.L. Self-assembly of stimuli-responsive block copolymers in aqueous solutions: An overview. *Polym. Bull.* **2020**, *77*, 5783–5810. [[CrossRef](#)]
13. Coppola, L.; Oliviero, C.; Pogliani, L.; Ranieri, G.A.; Terenzi, M. A self-diffusion study in aqueous solution and lyotropic mesophases of amphiphilic block copolymers. *Colloid Polym. Sci.* **2000**, *278*, 434–442. [[CrossRef](#)]
14. Wanka, G.; Hoffmann, H.; Ulbricht, W. Phase Diagrams and Aggregation Behavior of Poly(oxyethylene)-Poly(oxypropylene)-Poly(oxyethylene) Triblock Copolymers in Aqueous Solutions. *Macromolecules* **1994**, *27*, 4145–4159. [[CrossRef](#)]
15. Zhai, J.; Fan, B.; Thang, S.; Drummond, C. Novel Amphiphilic Block Copolymers for the Formation of Stimuli-Responsive Non-Lamellar Lipid Nanoparticles. *Molecules* **2021**, *26*, 3648. [[CrossRef](#)] [[PubMed](#)]
16. Zhang, K.; Khan, A. Phase Behavior of Poly(Ethylene Oxide)-Poly (Propylene Oxide)-Poly (Ethylene Oxide) Triblock Copolymers in Water. *Macromolecules* **1995**, *28*, 3807–3812. [[CrossRef](#)]
17. Tiwari, S.; Mall, C.; Prakash Solanki, P. Surfactant and Its Applications: A Review. *Int. J. Eng. Res. Appl.* **2018**, *8*, 61–66. [[CrossRef](#)]
18. Gustafsson, J.; Ljusberg-Wahren, H.; Almgren, M.; Larsson, K. Submicron Particles of Reversed Lipid Phases in Water Stabilized by a Nonionic Amphiphilic Polymer. *Langmuir* **1997**, *13*, 6964–6971. [[CrossRef](#)]
19. Gustafsson, J.; Ljusberg-Wahren, H.; Almgren, M.; Larsson, K. Cubic Lipid–Water Phase Dispersed into Submicron Particles. *Langmuir* **1996**, *12*, 4611–4613. [[CrossRef](#)]
20. De Campo, L.; Yaghmur, A.; Sagalowicz, L.; Leser, M.E.; Watzke, H.; Glatter, O. Reversible Phase Transitions in Emulsified Nanostructured Lipid Systems. *Langmuir* **2004**, *20*, 5254–5261. [[CrossRef](#)]
21. Larsson, K. Aqueous dispersions of cubic lipid–water phases. *Curr. Opin. Colloid Interface Sci.* **2000**, *5*, 64–69. [[CrossRef](#)]
22. Abraham, T.; Hato, M.; Hirai, M. Glycolipid based cubic nanoparticles: Preparation and structural aspects. *Colloids Surf. B Biointerfaces* **2004**, *35*, 107–118. [[CrossRef](#)] [[PubMed](#)]
23. Mele, S.; Murgia, S.; Monduzzi, M. Monoolein based liquid crystals to form long-term stable emulsions. *Colloids Surf. A Physicochem. Eng. Asp.* **2003**, *228*, 57–63. [[CrossRef](#)]
24. Spicer, P.T.; Hayden, K.L.; Lynch, M.L.; Ofori-Boateng, A.; Burns, J.L. Novel Process for Producing Cubic Liquid Crystalline Nanoparticles (Cubosomes). *Langmuir* **2001**, *17*, 5748–5756. [[CrossRef](#)]
25. Yaghmur, A.; de Campo, L.; Salentinig, S.; Sagalowicz, L.; Leser, M.E.; Glatter, O. Oil-Loaded Monolinolein-Based Particles with Confined Inverse Discontinuous Cubic Structure (Fd3m). *Langmuir* **2005**, *22*, 517–521. [[CrossRef](#)] [[PubMed](#)]

26. Kumar, H.; Sureshkumar, A.; Badduri, N.; Jain, V. A Review on Lyotropic Liquid Crystals and Its Potential Applications. *Nanosci. Nanotechnol. Asia* **2021**, *11*, 50–63. [[CrossRef](#)]
27. Monduzzi, M.; Ljusberg-Wahren, H.; Larsson, K. A ¹³C NMR Study of Aqueous Dispersions of Reversed Lipid Phases. *Langmuir* **2000**, *16*, 7355–7358. [[CrossRef](#)]
28. Larsson, K. Cubic lipid-water phases: Structures and biomembrane aspects. *J. Phys. Chem.* **1989**, *93*, 7304–7314. [[CrossRef](#)]
29. Rakotoarisoa, M.; Angelov, B.; Garamus, V.M.; Angelova, A. Curcumin- and Fish Oil-Loaded Spongosome and Cubosome Nanoparticles with Neuroprotective Potential against H₂O₂-Induced Oxidative Stress in Differentiated Human SH-SY5Y Cells. *ACS Omega* **2019**, *4*, 3061–3073. [[CrossRef](#)]
30. Yaghmur, A.; de Campo, L.; Sagalowicz, L.; Leser, M.E.; Glatter, O. Emulsified Microemulsions and Oil-Containing Liquid Crystalline Phases. *Langmuir* **2004**, *21*, 569–577. [[CrossRef](#)]
31. Kunieda, H.; Shigeta, K.; Nakamura, K.; Imae, T. Formation and structure of reverse vesicles. *Trends Colloid Interface Sci. X* **2007**, *100*, 1–5. [[CrossRef](#)]
32. Weiss, T.M.; Narayanan, T.; Gradzielski, M. Dynamics of Spontaneous Vesicle Formation in Fluorocarbon and Hydrocarbon Surfactant Mixtures. *Langmuir* **2008**, *24*, 3759–3766. [[CrossRef](#)] [[PubMed](#)]
33. Kunieda, H.; Akimaru, M.; Ushio, N.; Nakamura, K. Reverse Vesicles: Counter Structure of Biological Membranes. *J. Colloid Interface Sci.* **1993**, *156*, 446–453. [[CrossRef](#)]
34. Fischer, S.; Exner, A.; Zielske, K.; Perlich, J.; Deloudi, S.; Steurer, W.; Lindner, P.; Förster, S. Colloidal quasicrystals with 12-fold and 18-fold diffraction symmetry. *Proc. Natl. Acad. Sci. USA* **2011**, *108*, 1810–1814. [[CrossRef](#)]
35. Jayaraman, A.; Baez-Cotto, C.M.; Mann, T.J.; Mahanthappa, M.K. Dodecagonal quasicrystals of oil-swollen ionic surfactant micelles. *Proc. Natl. Acad. Sci. USA* **2021**, *118*, e2101598118. [[CrossRef](#)] [[PubMed](#)]
36. Griffin, W.C. Calculation of HLB Values of Non-Ionic Surfactants. *J. Soc. Cosmet. Chem.* **1954**, *5*, 249–256.
37. Griffin, W.C. Classification of Surface-Active Agents by “HLB”. *J. Soc. Cosmet. Chem.* **1949**, *1*, 311–326.
38. Guillot, S.; Salentinig, S.; Chemelli, A.; Sagalowicz, L.; Leser, M.E.; Glatter, O. Influence of the Stabilizer Concentration on the Internal Liquid Crystalline Order and the Size of Oil-Loaded Monolinolein-Based Dispersions. *Langmuir* **2010**, *26*, 6222–6229. [[CrossRef](#)]
39. Almgren, M.; Edwards, K.; Gustafsson, J. Cryotransmission electron microscopy of thin vitrified samples. *Curr. Opin. Colloid Interface Sci.* **1996**, *1*, 270–278. [[CrossRef](#)]
40. Barauskas, J.; Johnsson, M.; Joabsson, F.; Tiberg, F. Cubic Phase Nanoparticles (Cubosome): Principles for Controlling Size, Structure, and Stability. *Langmuir* **2005**, *21*, 2569–2577. [[CrossRef](#)]
41. Sagalowicz, L.; Michel, M.; Adrian, M.; Frossard, P.; Rouvet, M.; Watzke, H.J.; Yaghmur, A.; de Campo, L.; Glatter, O.; Leser, M.E. Crystallography of dispersed liquid crystalline phases studied by cryo-transmission electron microscopy. *J. Microsc.* **2006**, *221*, 110–121. [[CrossRef](#)]
42. Chong, J.; Mulet, X.; Waddington, L.J.; Boyd, B.J.; Drummond, C.J. High-Throughput Discovery of Novel Steric Stabilizers for Cubic Lyotropic Liquid Crystal Nanoparticle Dispersions. *Langmuir* **2012**, *28*, 9223–9232. [[CrossRef](#)] [[PubMed](#)]
43. Chong, J.Y.T.; Mulet, X.; Waddington, L.J.; Boyd, B.J.; Drummond, C.J. Steric stabilisation of self-assembled cubic lyotropic liquid crystalline nanoparticles: High throughput evaluation of triblock polyethylene oxide-polypropylene oxide-polyethylene oxide copolymers. *Soft Matter* **2011**, *7*, 4768–4777. [[CrossRef](#)]
44. Rodriguez, A.M.B.; Binks, B.P.; Sekine, T. Emulsion stabilisation by complexes of oppositely charged synthetic polyelectrolytes. *Soft Matter* **2018**, *14*, 239–254. [[CrossRef](#)] [[PubMed](#)]
45. Finkle, P.; Draper, H.D.; Hildebrand, J.H. The Theory of Emulsification1. *J. Am. Chem. Soc.* **1923**, *45*, 2780–2788. [[CrossRef](#)]
46. Larson-Smith, K.; Jackson, A.; Pozzo, D.C. SANS and SAXS Analysis of Charged Nanoparticle Adsorption at Oil–Water Interfaces. *Langmuir* **2012**, *28*, 2493–2501. [[CrossRef](#)]
47. Frelichowska, J.; Bolzinger, M.A.; Chevalier, Y. Effects of solid particle content on properties of o/w Pickering emulsions. *J. Colloid Interface Sci.* **2010**, *351*, 348–356. [[CrossRef](#)]
48. Binks, B.P.; Lumsdon, S.O. Pickering Emulsions Stabilized by Monodisperse Latex Particles: Effects of Particle Size. *Langmuir* **2001**, *17*, 4540–4547. [[CrossRef](#)]
49. Binks, B.P. Particles as surfactants—similarities and differences. *Curr. Opin. Colloid Interface Sci.* **2002**, *7*, 21–41. [[CrossRef](#)]
50. Binks, B.P.; Lumsdon, S.O. Stability of oil-in-water emulsions stabilised by silica particles. *Phys. Chem. Chem. Phys.* **1999**, *1*, 3007–3016. [[CrossRef](#)]
51. Aveyard, R.; Binks, B.P.; Clint, J.H. Emulsions stabilised solely by colloidal particles. *Adv. Colloid Interface Sci.* **2003**, *100*, 503–546. [[CrossRef](#)]
52. Ashby, N.P.; Binks, B.P. Pickering emulsions stabilised by Laponite clay particles. *Phys. Chem. Chem. Phys.* **2000**, *2*, 5640–5646. [[CrossRef](#)]
53. Sadeghpour, A.; Pirolt, F.; Iglesias, G.R.; Glatter, O. Lipid Transfer between Submicrometer Sized Pickering ISAsome Emulsions and the Influence of Added Hydrogel. *Langmuir* **2014**, *30*, 2639–2647. [[CrossRef](#)] [[PubMed](#)]
54. Sadeghpour, A.; Pirolt, F.; Glatter, O. Submicrometer-Sized Pickering Emulsions Stabilized by Silica Nanoparticles with Adsorbed Oleic Acid. *Langmuir* **2013**, *29*, 6004–6012. [[CrossRef](#)] [[PubMed](#)]

55. Muller, F.; Salonen, A.; Dulle, M.; Glatter, O. Salt-Induced Behavior of Internally Self-Assembled Nanodrops: Understanding Stabilization by Charged Colloids. In *Trends in Colloid and Interface Science XXIV*; Springer Science and Business Media LLC: Berlin/Heidelberg, Germany, 2011; pp. 27–31.
56. Salonen, A.; Muller, F.; Glatter, O. Internally Self-Assembled Submicrometer Emulsions Stabilized by Spherical Nanocolloids: Finding the Free Nanoparticles in the Aqueous Continuous Phase. *Langmuir* **2010**, *26*, 7981–7987. [[CrossRef](#)]
57. Muller, F.; Salonen, A.; Glatter, O. Phase behavior of Phytantriol/water bicontinuous cubic Pn3m cubosomes stabilized by Laponite disc-like particles. *J. Colloid Interface Sci.* **2010**, *342*, 392–398. [[CrossRef](#)]
58. Muller, F.; Salonen, A.; Glatter, O. Monoglyceride-based cubosomes stabilized by Laponite: Separating the effects of stabilizer, pH and temperature. *Colloids Surf. A Physicochem. Eng. Asp.* **2010**, *358*, 50–56. [[CrossRef](#)]
59. Salonen, A.; Muller, F.; Glatter, O. Dispersions of Internally Liquid Crystalline Systems Stabilized by Charged Disklike Particles as Pickering Emulsions: Basic Properties and Time-Resolved Behavior. *Langmuir* **2008**, *24*, 5306–5314. [[CrossRef](#)]
60. Sarkar, A.; Dickinson, E. Sustainable food-grade Pickering emulsions stabilized by plant-based particles. *Curr. Opin. Colloid Interface Sci.* **2020**, *49*, 69–81. [[CrossRef](#)]
61. Binks, B.P.; Muijlwijk, K.; Koman, H.; Poortinga, A.T. Food-grade Pickering stabilisation of foams by in situ hydrophobisation of calcium carbonate particles. *Food Hydrocoll.* **2017**, *63*, 585–592. [[CrossRef](#)]
62. Dickinson, E. Biopolymer-based particles as stabilizing agents for emulsions and foams. *Food Hydrocoll.* **2017**, *68*, 219–231. [[CrossRef](#)]
63. Zhu, F. Starch based Pickering emulsions: Fabrication, properties, and applications. *Trends Food Sci. Technol.* **2019**, *85*, 129–137. [[CrossRef](#)]
64. Linke, C.; Drusch, S. Pickering emulsions in foods—Opportunities and limitations. *Crit. Rev. Food Sci. Nutr.* **2018**, *58*, 1971–1985. [[CrossRef](#)] [[PubMed](#)]
65. Xiao, J.; Li, Y.; Huang, Q. Recent advances on food-grade particles stabilized Pickering emulsions: Fabrication, characterization and research trends. *Trends Food Sci. Technol.* **2016**, *55*, 48–60. [[CrossRef](#)]
66. Tavernier, I.; Wijaya, W.; Van der Meeren, P.; Dewettinck, K.; Patel, A.R. Food-grade particles for emulsion stabilization. *Trends Food Sci. Technol.* **2016**, *50*, 159–174. [[CrossRef](#)]
67. Dickinson, E. Food emulsions and foams: Stabilization by particles. *Curr. Opin. Colloid Interface Sci.* **2010**, *15*, 40–49. [[CrossRef](#)]
68. Jiao, J.; Burgess, D.J. Ostwald ripening of water-in-hydrocarbon emulsions. *J. Colloid Interface Sci.* **2003**, *264*, 509–516. [[CrossRef](#)]
69. Yarranton, H.W.; Hussein, H.; Masliyah, J.H. Water-in-Hydrocarbon Emulsions Stabilized by Asphaltenes at Low Concentrations. *J. Colloid Interface Sci.* **2000**, *228*, 52–63. [[CrossRef](#)]
70. Neto, D.M.C.; Sad, C.C.C.; Silva, M.; Santos, F.D.; Pereira, L.B.; Corona, R.R.; Silva, S.R.C.; Bassane, J.F.P.; Castro, E.V.R.; Lacerda, V., Jr.; et al. Rheological study of the behaviour of water-in-oil emulsions of heavy oils. *J. Pet. Sci.* **2019**, *173*, 1323–1331. [[CrossRef](#)]
71. Fingas, M.F. Water-in-Oil Emulsions: Formation and Prediction. *J. Pet. Sci. Res.* **2014**, *3*, 38. [[CrossRef](#)]
72. Fingas, M.; Fieldhouse, B. Studies of the formation process of water-in-oil emulsions. *Mar. Pollut. Bull.* **2003**, *47*, 369–396. [[CrossRef](#)]
73. Ushikubo, F.; Cunha, R. Stability mechanisms of liquid water-in-oil emulsions. *Food Hydrocoll.* **2014**, *34*, 145–153. [[CrossRef](#)]
74. Flak, D.K.; Adamski, V.; Nowaczyk, G.; Szutkowski, K.; Synowitz, M.; Jurga, S.; Held-Feindt, J. AT101-Loaded Cubosomes as an Alternative for Improved Glioblastoma Therapy. *Int. J. Nanomed.* **2020**, *15*, 7415–7431. [[CrossRef](#)] [[PubMed](#)]
75. Mahant, S.; Rao, R.; Souto, E.B.; Nanda, S. Analytical tools and evaluation strategies for nanostructured lipid carrier-based topical delivery systems. *Expert Opin. Drug Deliv.* **2020**, *17*, 963–992. [[CrossRef](#)]
76. Faria, A.R.; Silvestre, O.; Maibohm, C.; Adão, R.; Silva, B.; Nieder, J.B. Cubosome nanoparticles for enhanced delivery of mitochondria anticancer drug elesclomol and therapeutic monitoring via sub-cellular NAD(P)H multi-photon fluorescence lifetime imaging. *Nano Res.* **2018**, *12*, 991–998. [[CrossRef](#)]
77. Zhai, J.; Tan, F.H.; Luwor, R.B.; Srinivasa Reddy, T.; Ahmed, N.; Drummond, C.J.; Tran, N. In Vitro and In Vivo Toxicity and Biodistribution of Paclitaxel-Loaded Cubosomes as a Drug Delivery Nanocarrier: A Case Study Using an A431 Skin Cancer Xenograft Model. *ACS Appl. Bio Mater.* **2020**, *3*, 4198–4207. [[CrossRef](#)]
78. Zhai, J.; Fong, C.; Tran, N.; Drummond, C.J. Non-Lamellar Lyotropic Liquid Crystalline Lipid Nanoparticles for the Next Generation of Nanomedicine. *ACS Nano* **2019**, *13*, 6178–6206. [[CrossRef](#)]
79. Bor, G.; Azmi, I.D.M.; Yaghmur, A. Nanomedicines for cancer therapy: Current status, challenges and future prospects. *Ther. Deliv.* **2019**, *10*, 113–132. [[CrossRef](#)]
80. Prajapati, R.; Larsen, S.W.; Yaghmur, A. Citrem—Phosphatidylcholine nano-self-assemblies: Solubilization of bupivacaine and its role in triggering a colloidal transition from vesicles to cubosomes and hexosomes. *Phys. Chem. Chem. Phys.* **2019**, *21*, 15142–15150. [[CrossRef](#)]
81. Azmi, I.D.M.; Østergaard, J.; Stürup, S.; Gammelgaard, B.; Urtti, A.; Moghimi, S.M.; Yaghmur, A. Cisplatin Encapsulation Generates Morphologically Different Multicompartment in the Internal Nanostructures of Nonlamellar Liquid-Crystalline Self-Assemblies. *Langmuir* **2018**, *34*, 6570–6581. [[CrossRef](#)]
82. García-Pinel, B.; Porras-Alcalá, C.; Ortega-Rodríguez, A.; Sarabia, F.; Prados, J.; Melguizo, C.; López-Romero, J.M. Lipid-Based Nanoparticles: Application and Recent Advances in Cancer Treatment. *Nanomaterials* **2019**, *9*, 638. [[CrossRef](#)] [[PubMed](#)]

83. Tajik-Ahmadabad, B.; Chollet, L.; White, J.; Separovic, F.; Polyzos, A. Metallo-Cubosomes: Zinc-Functionalized Cubic Nanoparticles for Therapeutic Nucleotide Delivery. *Mol. Pharm.* **2019**, *16*, 978–986. [[CrossRef](#)] [[PubMed](#)]
84. Azmi, I.D.; Moghimi, S.M.; Yaghmur, A. Cubosomes and hexosomes as versatile platforms for drug delivery. *Ther. Deliv.* **2015**, *6*, 1347–1364. [[CrossRef](#)] [[PubMed](#)]
85. Barriga, H.M.G.; Holme, M.N.; Stevens, M.M. Cubosomes: The Next Generation of Smart Lipid Nanoparticles? *Angew. Chem. Int. Ed.* **2019**, *58*, 2958–2978. [[CrossRef](#)]
86. Yingchoncharoen, P.; Kalinowski, D.S.; Richardson, D.R. Lipid-Based Drug Delivery Systems in Cancer Therapy: What Is Available and What Is Yet to Come. *Pharmacol. Rev.* **2016**, *68*, 701–787. [[CrossRef](#)]
87. Zabara, M.; Senturk, B.; Gontsarik, M.; Ren, Q.; Rottmar, M.; Maniura, K.; Mezzenga, R.; Bolisetty, S.; Salentinig, S. Multifunctional Nano-Biointerfaces: Cytocompatible Antimicrobial Nanocarriers from Stabilizer-Free Cubosomes. *Adv. Funct. Mater.* **2019**, *29*, 1904007. [[CrossRef](#)]
88. Chemelli, A.; Conde-Valentín, B.; Uhlig, F.; Glatter, O. Amino Acid Induced Modification of Self-Assembled Monoglyceride-Based Nanostructures. *Langmuir* **2015**, *31*, 10377–10381. [[CrossRef](#)]
89. Chemelli, A.; Maurer, M.; Geier, R.; Glatter, O. Optimized Loading and Sustained Release of Hydrophilic Proteins from Internally Nanostructured Particles. *Langmuir* **2012**, *28*, 16788–16797. [[CrossRef](#)]
90. Mehata, A.K.; Dehari, D.; Gupta, A.; Rabin, D.C.; Miya, A. Multifunctional Liquid Crystal Nanoparticles for Cancer Therapy. *Curr. Nanomater.* **2021**, *6*, 4–16. [[CrossRef](#)]
91. Mohammad, Y.; Prentice, R.N.; Boyd, B.J.; Rizwan, S.B. Comparison of cubosomes and hexosomes for the delivery of phenytoin to the brain. *J. Colloid Interface Sci.* **2021**, *605*, 146–154. [[CrossRef](#)]
92. Millart, E.; Lesieur, S.; Faivre, V. Superparamagnetic lipid-based hybrid nanosystems for drug delivery. *Expert Opin. Drug Deliv.* **2018**, *15*, 523–540. [[CrossRef](#)] [[PubMed](#)]
93. Tien, N.D.; Maurya, A.K.; Fortunato, G.; Rottmar, M.; Zboray, R.; Erni, R.; Dommann, A.; Rossi, R.M.; Neels, A.; Sadeghpour, A. Responsive Nanofibers with Embedded Hierarchical Lipid Self-Assemblies. *Langmuir* **2020**, *36*, 11787–11797. [[CrossRef](#)] [[PubMed](#)]
94. Gontsarik, M.; Yaghmur, A.; Ren, Q.; Maniura-Weber, K.; Salentinig, S. From Structure to Function: pH-Switchable Antimicrobial Nano-Self-Assemblies. *ACS Appl. Mater. Interfaces* **2019**, *11*, 2821–2829. [[CrossRef](#)] [[PubMed](#)]
95. Gontsarik, M.; Mohammadtaheri, M.; Yaghmur, A.; Salentinig, S. pH-Triggered nanostructural transformations in antimicrobial peptide/oleic acid self-assemblies. *Biomater. Sci.* **2018**, *6*, 803–812. [[CrossRef](#)] [[PubMed](#)]
96. Li, Y.; Angelova, A.; Hu, F.; Garamus, V.M.; Peng, C.; Li, N.; Liu, J.; Liu, D.; Zou, A. pH Responsiveness of Hexosomes and Cubosomes for Combined Delivery of *Brucea javanica* Oil and Doxorubicin. *Langmuir* **2019**, *35*, 14532–14542. [[CrossRef](#)] [[PubMed](#)]
97. Prajapati, R.; Gontsarik, M.; Yaghmur, A.; Salentinig, S. pH-Responsive Nano-Self-Assemblies of the Anticancer Drug 2-Hydroxyoleic Acid. *Langmuir* **2019**, *35*, 7954–7961. [[CrossRef](#)]
98. Mathews, P.D.; Mertins, O.; Angelov, B.; Angelova, A. Cubosomal lipid nanoassemblies with pH-sensitive shells created by biopolymer complexes: A synchrotron SAXS study. *J. Colloid Interface Sci.* **2021**, *607*, 440–450. [[CrossRef](#)]
99. Mertins, O.; Mathews, P.D.; Angelova, A. Advances in the Design of pH-Sensitive Cubosome Liquid Crystalline Nanocarriers for Drug Delivery Applications. *Nanomaterials* **2020**, *10*, 963. [[CrossRef](#)]
100. Boyd, B.J. Characterisation of drug release from cubosomes using the pressure ultrafiltration method. *Int. J. Pharm.* **2003**, *260*, 239–247. [[CrossRef](#)]
101. Pucek, A.; Tokarek, B.; Waglewska, E.; Bazylińska, U. Recent Advances in the Structural Design of Photosensitive Agent Formulations Using “Soft” Colloidal Nanocarriers. *Pharmaceutics* **2020**, *12*, 587. [[CrossRef](#)]
102. Tomšič, M.; Guillot, S.; Sagalowicz, L.; Leser, M.E.; Glatter, O. Internally Self-Assembled Thermoreversible Gelling Emulsions: ISAsomes in Methylcellulose, κ -Carrageenan, and Mixed Hydrogels. *Langmuir* **2009**, *25*, 9525–9534. [[CrossRef](#)] [[PubMed](#)]
103. Caselli, L.; Mendoza, M.; Muzzi, B.; Toti, A.; Montis, C.; Mello, T.; Mannelli, L.D.C.; Ghelardini, C.; Sangregorio, C.; Berti, D. Lipid Cubic Mesophases Combined with Superparamagnetic Iron Oxide Nanoparticles: A Hybrid Multifunctional Platform with Tunable Magnetic Properties for Nanomedical Applications. *Int. J. Mol. Sci.* **2021**, *22*, 9268. [[CrossRef](#)] [[PubMed](#)]
104. Salentinig, S.; Sagalowicz, L.; Leser, M.E.; Tedeschi, C.; Glatter, O. Transitions in the internal structure of lipid droplets during fat digestion. *Soft Matter* **2010**, *7*, 650–661. [[CrossRef](#)]
105. Salentinig, S.; Amenitsch, H.; Yaghmur, A. In Situ Monitoring of Nanostructure Formation during the Digestion of Mayonnaise. *ACS Omega* **2017**, *2*, 1441–1446. [[CrossRef](#)]
106. Salentinig, S. Supramolecular structures in lipid digestion and implications for functional food delivery. *Curr. Opin. Colloid Interface Sci.* **2019**, *39*, 190–201. [[CrossRef](#)]
107. Salentinig, S.; Phan, S.; Hawley, A.; Boyd, B.J. Self-Assembly Structure Formation during the Digestion of Human Breast Milk. *Angew. Chem. Int. Ed.* **2015**, *54*, 1600–1603. [[CrossRef](#)]
108. Mezzenga, R.; Schurtenberger, P.; Burbidge, A.; Michel, M. Understanding foods as soft materials. *Nat. Mater.* **2005**, *4*, 729–740. [[CrossRef](#)]
109. Krog, N. *Emulsifiers and Emulsions in Dairy Foods*; Elsevier: Amsterdam, The Netherlands, 2002; pp. 891–900.
110. Larsson, K. Lyotropic liquid crystals and their dispersions relevant in foods. *Curr. Opin. Colloid Interface Sci.* **2009**, *14*, 16–20. [[CrossRef](#)]
111. Ubbink, J.; Mezzenga, R. Delivery of functionality in complex food systems: Introduction. *Trends Food Sci. Technol.* **2006**, *17*, 194–195. [[CrossRef](#)]

112. Yaghmur, A. Nanoencapsulation of food ingredients by cubosomes and hexosomes. In *Lipid-Based Nanostructures for Food Encapsulation Purposes*; Academic Press: Cambridge, MA, USA, 2019; pp. 483–522. [[CrossRef](#)]
113. Garti, N.; Clement, V.; Fanun, M.; Leser, M.E. Some Characteristics of Sugar Ester Nonionic Microemulsions in View of Possible Food Applications. *J. Agric. Food Chem.* **2000**, *48*, 3945–3956. [[CrossRef](#)]
114. Fornasier, M.; Pireddu, R.; Del Giudice, A.; Sinico, C.; Nylander, T.; Schillén, K.; Galantini, L.; Murgia, S. Tuning lipid structure by bile salts: Hexosomes for topical administration of catechin. *Colloids Surf. B Biointerfaces* **2021**, *199*, 111564. [[CrossRef](#)] [[PubMed](#)]
115. Aditya, N.; Espinosa, Y.G.; Norton, I.T. Encapsulation systems for the delivery of hydrophilic nutraceuticals: Food application. *Biotechnol. Adv.* **2017**, *35*, 450–457. [[CrossRef](#)] [[PubMed](#)]
116. Sadeghpour, M.R.A. Lyotropic Liquid Crystalline Phases for the Formulation of Future Functional Foods. *J. Nutr. Health Food Eng.* **2016**, *5*, 1–5. [[CrossRef](#)]
117. Cortesi, R.; Cappellozza, E.; Drechsler, M.; Contado, C.; Baldisserotto, A.; Mariani, P.; Carducci, F.; Pecorelli, A.; Esposito, E.; Valacchi, G. Monoolein aqueous dispersions as a delivery system for quercetin. *Biomed. Microdevices* **2017**, *19*, 41. [[CrossRef](#)] [[PubMed](#)]
118. Chatzidakis, M.D.; Mitsou, E.; Yaghmur, A.; Xenakis, A.; Papadimitriou, V. Formulation and characterization of food-grade microemulsions as carriers of natural phenolic antioxidants. *Colloids Surf. A Physicochem. Eng. Asp.* **2015**, *483*, 130–136. [[CrossRef](#)]
119. Rafiee, Z.; Nejatian, M.; Daeihamed, M.; Jafari, S.M. Application of different nanocarriers for encapsulation of curcumin. *Crit. Rev. Food Sci. Nutr.* **2019**, *59*, 3468–3497. [[CrossRef](#)]
120. Serieye, S.; Méducin, F.; Tidu, A.; Guillot, S. Incorporation of aromas in nanostructured monolinolein-based miniemulsions: A structural investigation. *Colloids Surf. A Physicochem. Eng. Asp.* **2018**, *555*, 802–808. [[CrossRef](#)]
121. Rezaei, A.; Fathi, M.; Jafari, S.M. Nanoencapsulation of hydrophobic and low-soluble food bioactive compounds within different nanocarriers. *Food Hydrocoll.* **2019**, *88*, 146–162. [[CrossRef](#)]
122. Evans, D.F.; Pye, G.; Bramley, R.; Clark, A.G.; Dyson, T.J.; Hardcastle, J.D. Measurement of gastrointestinal pH profiles in normal ambulant human subjects. *Gut* **1988**, *29*, 1035–1041. [[CrossRef](#)]
123. Beasley, D.; Koltz, A.M.; Lambert, J.E.; Fierer, N.; Dunn, R. The Evolution of Stomach Acidity and Its Relevance to the Human Microbiome. *PLoS ONE* **2015**, *10*, e0134116. [[CrossRef](#)]
124. Glatter, O.; Glatter, I. Water-in-Oil Emulsions and Methods for Their Preparation. European Patent EP 2604253 2011, 9 November 2016.
125. Kulkarni, C.V.; Mezzenga, R.; Glatter, O. Water-in-oil nanostructured emulsions: Towards the structural hierarchy of liquid crystalline materials. *Soft Matter* **2010**, *6*, 5615–5624. [[CrossRef](#)]
126. Sreedharan, R.; Chidambaram, K. Drug/Vehicle Impacts and Formulation Centered Stratagems for Enhanced Transdermal Drug Permeation, Controlled Release and Safety: Unparalleled Past and Recent Innovations-An Overview. *Curr. Drug Ther.* **2019**, *14*, 192–209. [[CrossRef](#)]
127. Reis, P.; Holmberg, K.; Watzke, H.; Leser, M.; Miller, R. Lipases at interfaces: A review. *Adv. Colloid Interface Sci.* **2009**, *147*, 237–250. [[CrossRef](#)] [[PubMed](#)]
128. Moitzi, C.; Guillot, S.; Fritz, G.; Salentinig, S.; Glatter, O. Phase Reorganization in Self-Assembled Systems through Interparticle Material Transfer. *Adv. Mater.* **2007**, *19*, 1352–1358. [[CrossRef](#)]
129. Salonen, A.; Moitzi, C.; Salentinig, S.; Glatter, O. Material Transfer in Cubosome–Emulsion Mixtures: Effect of Alkane Chain Length. *Langmuir* **2010**, *26*, 10670–10676. [[CrossRef](#)] [[PubMed](#)]
130. Pirolt, F.; Glatter, O.; Trimmel, G. Reverse Hexosome Dispersions in Alkanes—The Challenge of Inverting Structures. *Langmuir* **2018**, *34*, 8379–8387. [[CrossRef](#)]
131. Hassan, T.; Mäder, K.; Maeder, K. Novel semisolid SNEDDS based on PEG-30-di-(polyhydroxystearate): Progesterone incorporation and in vitro digestion. *Int. J. Pharm.* **2015**, *486*, 77–87. [[CrossRef](#)]
132. Milinkovic, J.; Petrovic, L.; Fraj, J.; Bučko, S.; Katona, J. Characteristics of W/O emulsions containing polymeric emulsifier PEG 30-dipolyhydroxystearate. *Acta Period. Technol.* **2016**, *47*, 219–230. [[CrossRef](#)]
133. Koppel, D.E. Analysis of Macromolecular Polydispersity in Intensity Correlation Spectroscopy: The Method of Cumulants. *J. Chem. Phys.* **1972**, *57*, 4814–4820. [[CrossRef](#)]
134. Alam, M.M.; Aramaki, K. Hexagonal Phase Based Gel-Emulsion (O/H1Gel-Emulsion): Formation and Rheology. *Langmuir* **2008**, *24*, 12253–12259. [[CrossRef](#)]
135. Mariani, P.; Luzzati, V.; Delacroix, H. Cubic phases of lipid-containing systems: Structure analysis and biological implications. *J. Mol. Biol.* **1988**, *204*, 165–189. [[CrossRef](#)]
136. Papadimitriou, V.; Dulle, M.; Wachter, W.; Sotiroidis, T.G.; Glatter, O.; Xenakis, A. Structure and Dynamics of Veiled Virgin Olive Oil: Influence of Production Conditions and Relation to its Antioxidant Capacity. *Food Biophys.* **2013**, *8*, 112–121. [[CrossRef](#)]